



Enhanced isotopic approach combined with microbiological analyses for more precise distinction of various N-transformation processes in contaminated aquifer – a groundwater incubation study

Sushmita Deb¹, Mikk Espenberg², Reinhard Well³, Michal Bucha¹, Marta Jakubiak¹, Ülo Mander², Dominika Lewicka-Szczebak¹

¹ Institute of Geological Sciences, University of Wrocław, Poland

² Institute of Ecology and Earth Sciences, University of Tartu, Estonia

³ Thünen Institute of Climate-Smart Agriculture, Braunschweig, Germany

Correspondence to: Sushmita Deb (sushmita.deb@uwr.edu.pl)

Abstract

This study explores nitrogen transformations in groundwater from an agricultural area utilizing organic fertilizer (wastewaters from yeast production) integrating isotopic analysis, microbial gene abundance, and the FRAME (isotope FRactionation And Mixing Evaluation) model to trace and quantify nitrogen cycling pathways. Groundwater samples with elevated nitrate concentrations were subjected to controlled laboratory incubations with application of a novel low-level ¹⁵N tracing strategy, to investigate microbial processes. Isotope analyses of nitrate, nitrite and nitrous oxide (N₂O), coupled with microbial gene quantification via quantitative PCR (qPCR), revealed a shift from archaeal-driven nitrification to bacterial denitrification in post-incubation suboxic conditions, stimulated by glucose addition. FRAME modeling further identified bacterial denitrification (bD) as the dominant pathway of N₂O production, which was supported by increased *nosZI*, *nirK* and *nirS* gene abundance and observed isotope effects.

Simultaneously to the intensive nitrate reduction, it was observed that the majority of nitrite is likely produced through nitrification processes linked to dissolved organic nitrogen (DON) oxidation. Nitrate reduction had minor contribution in the total nitrite pool. The results demonstrate the efficacy of integrating multi-compound isotope studies and microbial analyses to unravel nitrogen cycling mechanisms. This approach provides a robust framework for addressing nitrogen pollution in groundwater systems and improving water quality management strategies.

Keywords

Denitrification pathways, $\delta^{15}\text{N}$ and $\delta^{18}\text{O}$ isotopes, nitrate, nitrite, N₂O, microbial gene abundance, FRAME modeling, agricultural pollution,

Introduction

Nitrogen (N) is an essential nutrient for plant growth and global food production, forming a key component of nucleic acids and proteins. Although synthetic N fertilizers containing nitrate (NO₃⁻) and/or ammonium (NH₄⁺), have greatly influenced agricultural yields, their excessive use has significantly disrupted the N cycle, leading to NO₃⁻ leaching in groundwater, emission of ammonia (NH₃), and gaseous forms of nitrogen oxides (nitric oxide (NO), nitrous oxide (N₂O), nitrogen dioxide (NO₂) which are of environmental concern (Sainju et al., 2020). These issues contribute to eutrophication of lakes, groundwater quality degradation, and greenhouse gas emissions, with N₂O intensifying global warming and ozone depletion (Butterbach-Bahl et al., 2013). Controlling



46 NO_3^- levels in aquatic systems presents substantial environmental challenges, particularly in
47 groundwater, due to the complexity of differentiating between its anthropogenic sources and
48 natural processes. Hence, the better understanding of N cycling is crucial to develop effective
49 solutions of environmental problems (Rütting et al., 2018).

50 Diverse microbial communities, including nitrogen-fixing bacteria, archaea, anammox bacteria,
51 nitrifiers, and denitrifiers, drive key N transformations, regulating its availability and mobility in
52 ecosystems. N undergoes complex transformation processes like nitrification, denitrification,
53 anammox, mineralization and immobilization (Deb et al., 2024) which regulate N availability to
54 plants and influence its movement in agricultural and natural systems. Biological fixation converts
55 atmospheric nitrogen (N_2) into bioavailable forms, while nitrification involves the microbial
56 oxidation of NH_4^+ to NO_3^- via nitrite (NO_2^-). Denitrification reduces NO_3^- to N_2 through the
57 intermediates NO_2^- , NO and N_2O . Depending on environmental conditions, this reduction may be
58 incomplete, leading to N_2O emissions. Moreover, the anammox or feammox processes converts
59 NH_4^+ and NO_2^- to N_2 (Ding et al., 2022; Einsiedl et al., 2020). These processes are interconnected
60 and influenced by environmental conditions, making it challenging to differentiate between the
61 sources and pathways of N transformations (Nikolenko et al., 2018). Further, functional
62 characterization of genes encoding key enzymes in N metabolism provides insights into the genetic
63 potential for specific transformations (Levy-Booth et al., 2014), while microbial community
64 structure analysis helps elucidate the physiological activities and ecological roles of microbes in
65 driving N transformations. Together, these approaches contribute to a comprehensive
66 understanding of N cycling processes.

67
68 Stable isotope studies help in tracing the N sources and transformations, through isotopic
69 signatures such as $\delta^{15}\text{N}$ and $\delta^{18}\text{O}$ in NO_3^- , NO_2^- , NH_4^+ , and N_2O (Denk et al., 2017, Deb et al.,
70 2024). However, limitations arise due to overlapping ranges of different isotope sources or
71 difficulty in distinction between isotope fractionation processes and mixing. To overcome such
72 limitations and enhance interpretations based on stable isotope studies a multi-compound analysis
73 approach can be applied (Well et al., 2012, Deb et al., 2024). Such multi-compound isotope
74 analysis provides a broader perspective on N cycle processes by examining multiple N-compounds
75 e.g., in denitrification $\delta^{15}\text{N}$ and $\delta^{18}\text{O}$ analysis of NO_3^- helps identify substrates, while NO_2^- and
76 N_2O analyses provide insight into intermediate products.

77 Since the range of natural isotope variations is relatively narrow, even analyses of multiple
78 compounds may provide ambiguous results. ^{15}N tracing technique allows for precise tracing of
79 artificially added N in the environment (Müller et al., 2004) but is spatially and temporally limited
80 and disrupts natural abundance isotope studies (Buchen-Tschiskale et al., 2023; Well et al., 2019),
81 which are easily and universally applicable in unmodified environmental conditions. A major
82 drawback of traditional ^{15}N tracing methods is the necessary sacrifice of other isotope tracers, such
83 as O isotope signatures and site preference values of N_2O , which cannot be accurately determined
84 when high ^{15}N additions are applied. This research introduces a novel approach using low-level
85 ^{15}N labelling, where a minimal amount of ^{15}N -labelled substrate is added to slightly increase $\delta^{15}\text{N}$
86 values (up to ca. 100-200‰) of a single substrate while maintaining the natural abundance levels.
87 This ensures that isotope fractionation remains relevant, and standard measurement methods for
88 all isotope signatures can still be applied. If the level of ^{15}N labelling exceeds the natural variability
89 of N sources and isotope fractionation effects, this approach enables clear distinction between
90 substrates involved in N transformations. It also allows for precise tracing of the path of N from



91 substrate to product while utilizing or determining isotope fractionation factors, which remain
92 applicable to natural abundance isotope studies in natural environments.

93 While stable isotope analysis provides valuable insights into nitrogen pathways, its interpretation
94 is often complicated by overlapping fractionation effects (Deb et al., 2024). To refine process
95 identification, microbiological approaches such as quantitative PCR (qPCR) enable the detection
96 and quantification of key genes involved in nitrogen transformations, providing insights into
97 microbial activity (Espenberg et al., 2018; Rohe et al., 2020).

98 However, these microbiological methods only reveal the potential for microbial species to
99 participate in nitrogen cycling rather than directly quantifying transformation rates. The detection
100 of functional genes or gene expression does not confirm whether a process is actively occurring at
101 a given time or its relative contribution within a system (Espenberg et al., 2018; Rohe et al.,
102 2020). Thus, combining stable isotope data with microbiological analyses enhances the precision of
103 nitrogen flux assessments in groundwater, offering a robust framework for tracing, quantifying,
104 and characterizing nitrogen transformations in complex environmental systems. The integration of
105 isotopic and microbial techniques for partitioning N cycle processes provided valuable insights
106 into N₂O source apportioning (MASTA et al., 2024).

107 Here we combine the isotope studies, applying novel low-labelling technique and multicomponent
108 analyses, with microbiological analyses using quantitative PCR (qPCR), which identify and
109 quantify key genes involved in N processes. This aims at better understanding of the occurring N
110 transformations and enhancement the precision of nitrogen flux assessments in groundwater.

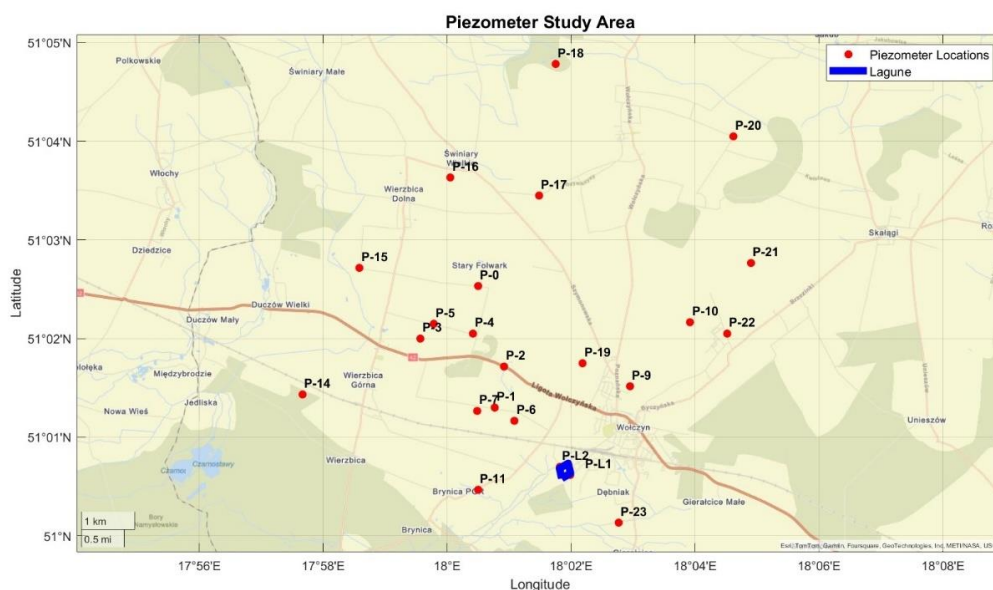
111

112 **2. Materials and Methods**

113 **2.1. Experimental Site**

114 Experiments were conducted from the groundwaters collected in an agricultural area near
115 Wólczyn, Poland, approximately 80 km north of Wrocław. On these crop fields wastewater from
116 a yeast factory is applied as a natural fertilizer, containing 300 mg L⁻¹ of TN (total nitrogen) and
117 835 mg L⁻¹ of TP (total potassium). While this approach supports agricultural production by
118 reducing reliance on synthetic fertilizers, it is likely to have a significant impact on groundwater
119 quality, especially by increasing N and P load. Preliminary sampling from piezometers in the study
120 area conducted on July 2023 revealed nitrate concentrations exceeding 80 mg L⁻¹ in the
121 groundwater, raising concerns about elevated nitrate levels, exceeding the norms for drinking
122 water of 50 mg L⁻¹. The following map (Fig. 1) illustrates the study area of our experiment,
123 highlighting the locations of piezometers used for groundwater sampling.

124



125

126

127

Figure 1: Piezometer Study Area near Wolczyn, Poland (Blue-marked area indicates the lagune for yeast-production sewage storage).

128

129

130

131

132

133

134

135

136

137

2.2. Water Sampling

138

139

140

141

142

143

144

145

146

147

148

149

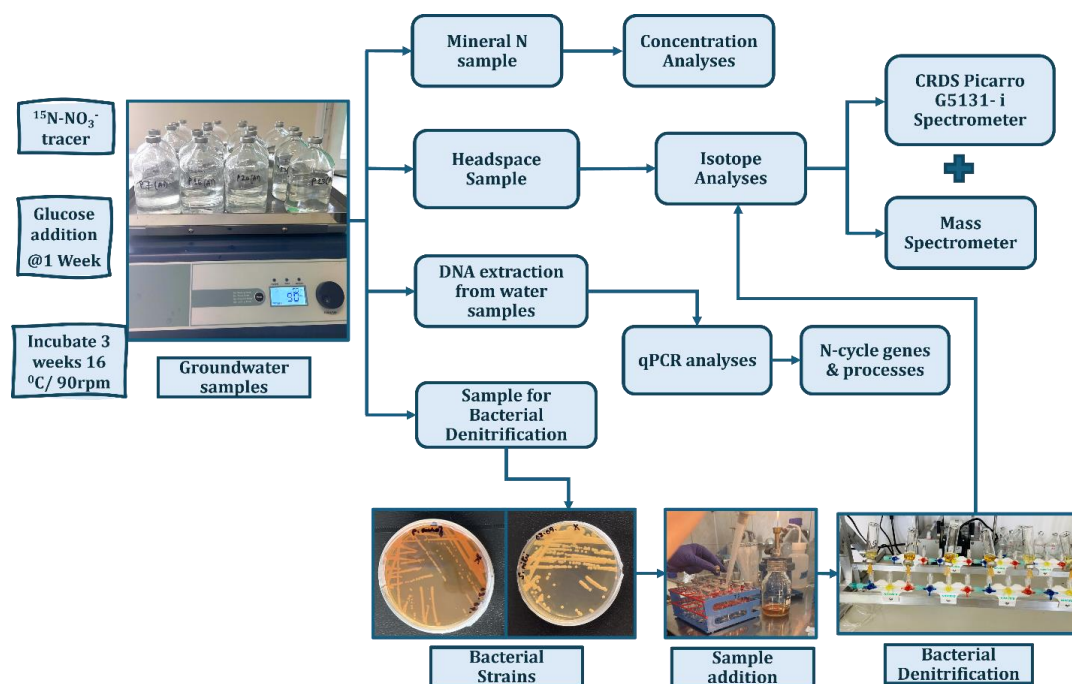
Groundwater samples from 23 piezometers in the study area were pumped out at varying depths during the field sampling campaign on 5th September 2023 (Table 1). Subsequently, water from four selected piezometers (P-7, P-16, P-20, P-23) were used for laboratory incubation studies to evaluate the potential N transformation processes and identify the isotope effects associated with them.



150 **Table 1: Concentrations of Nitrogen Species and Environmental Parameters in**
 151 **Groundwater Samples** (P abbreviated for piezometer), bd – below detection, piezometers
 152 selected for incubation – in bold font.
 153

Sam ple	Te mp er at ure (°C)	pH	Condu ctivity ($\mu\text{S cm}^{-1}$)	Nitra te (N- NO ₃ ⁻) (mg N L ⁻¹)	Nitrite (N- NO ₂ ⁻) (mg N L ⁻¹)	Ammon ium (N- NH ₄ ⁺) (mg N L ⁻¹)	DOC (dissol ved organi c carbo n) (mg C L ⁻¹)	DON (dissol ved organi c nitro gen) (mgN L ⁻¹)	$\delta^{15}\text{N}$		$\delta^{18}\text{O}$	
									$\delta^{15}\text{N-NO}_3^-$	$\delta^{15}\text{N-NO}_2^-$	$\delta^{18}\text{O-NO}_3^-$	$\delta^{18}\text{O-NO}_2^-$
P-0	13.5	6.5	928	39.65	0.08	0.33	24.12	32.76	0.9	-31.0	0.5	bd
P-1	14	6.1	1000	21.05	0.284	0.224	42.06	16.76	7.7	-27.8	6.1	-7.3
P-2	13.4	7.3	1245	0.62	0.21	7.05	67.42	bd	bd	bd	bd	bd
P-3	14.1	6.7	998	39.3	0.405	0.316	27.28	57.08	4.3	-30.2	0.4	-4.2
P-4	12.8	7.3	4794	0.63	0.398	11.46	431.3	7.74	bd	bd	bd	bd
P-5	13.5	6.8	1030	18.45	0.092	0.103	176.9	6.12	9.3	bd	3.3	bd
P-6	17	7.5	1386	0.24	0.034	0.31	58.42	bd	bd	bd	bd	bd
P-7	13.2	6.9	1395	32.8	0.188	0.138	46.32	41.04	6.6	-37.0	3.2	8.5
P-9	14.4	6.7	919	0.11	<0	0.17	52.59	bd	bd	bd	bd	bd
P-10	12.2	6.8	944	0.98	0.02	1.509	24.66	bd	10.4	bd	6.1	bd
P-11	14.2	7.3	1343	0.5	0.081	2.33	bd	bd	bd	bd	bd	bd
P-14	15.5	7.1	845	0.33	0.114	14.98	bd	bd	bd	bd	bd	bd
P-15	14.7	7	512	0.44	0.146	4.397	22.28	bd	bd	bd	bd	bd
P-16	10	6.2	617	39.45	0.098	0.031	10.22	31.88	3.7	-17.3	1.6	4.4
P-17	12.7	7.1	685	0.26	0.018	0.557	51.81	bd	bd	bd	bd	bd
P-18	11.2	7.1	560	1.8	0.06	0.651	55.85	bd	8.4	bd	7.7	bd
P-19	13.9	6.6	617	0.52	0.025	0.611	9.23	bd	bd	bd	bd	bd
P-20	11.1	6.6	471	38.12	0.019	0.028	9.7	30.63	1.0	bd	-0.9	bd
P-21	10.9	7.1	574	0.43	0.087	0.565	31.49	bd	bd	bd	bd	bd
P-22	11.1	5.6	557	2.47	0.064	0.215	14.81	5.01	16.0	bd	4.8	bd
P-23	14.9	6.3	1238	89.5	0.354	0.059	21.22	91.72	5.3	-27.9	4.7	-8.9
P-L1	14.2	6.8	2581	1.26	0.226	0.817	262.4	69.28	10.3	5.4	1.9	15.7
P-L2	13.8	7	1777	0.2	0.058	17.95	68.9	25.74	bd	bd	bd	bd

154



155
156
157
158
159
160
161
162
163
164
165
166
167
168
169
170
171
172
173
174
175
176
177
178
179
180

Figure 2: Experimental Setup for microbial analyses (qPCR, Groundwater Incubation) and Isotopic Analysis. The scheme illustrates the workflow for analyzing groundwater samples, including incubation with $^{15}\text{N-NO}_3^-$ tracer, bacterial denitrification, DNA extraction, concentration analyses, and isotope measurements using a CRDS (Cavity Ring Down Spectroscopy) Picarro G5131-i spectrometer and mass spectrometer.

For inorganic N concentration and isotopic analyses, all groundwater samples were filtered using $0.45\ \mu\text{m}$ filters. For NO_3^- and NH_4^+ analysis, 50 ml of the filtered sample was collected in a Falcon tube, which was stored frozen until further analysis. For NO_2^- analysis, an additional 50 ml of the sample was collected in a separate Falcon tube, where after filtering 1 mL of 2 M KOH was added to raise the pH to 10-12, inhibiting nitrite reduction. The samples were then stored at $4\ ^\circ\text{C}$ until further analysis. It is essential to analyze these samples as soon as possible after collection to prevent microbial degradation and ensure data integrity.

From the field sampling 4 selected samples with high nitrate concentration were used for filtering and further microbial analyses. The field groundwater samples were immediately transported to the laboratory in an ice-cooled box and filtered using $0.45\ \mu\text{m}$ filters. For laboratory incubation studies, 2 L of groundwater from selected piezometers with high nitrate concentration were collected into sterile bottles and immediately sealed for a series of laboratory experiments, and stored frozen until further analysis. Further, from the later incubation studies (as described in 2.5), the water samples (600 ml from each incubated piezometers) were filtered using sterile $0.45\ \mu\text{m}$ filters for the further microbial analyses after the 3 week incubations period.



181 **2.3. Inorganic nitrogen analyses (NO_3^- , NO_2^- , NH_4^+) Using a Colorimetric Method**

182 For the analysis of NO_3^- , NO_2^- , and NH_4^+ concentrations, groundwater samples were filtered using
183 0.45 μm filters and measured with the SLANDI Photometer LF300 (Slandi Sp. z o.o.,
184 Michałowice, Poland), a versatile instrument for water and wastewater analysis across
185 wavelengths ranging from 380 nm to 810 nm. For our analysis, wavelengths of 520 nm, 560 nm,
186 and 610 nm were selected for NO_3^- , NO_2^- , and NH_4^+ concentration, respectively. Following a
187 standardized protocol, specific reagents were added to the samples, allowing the reactions to
188 develop colour and the concentrations were then measured photometrically.

189
190 **2.4. Inorganic nitrogen isotope analyses**

191 To trace microbial N transformations processes in the groundwater samples, inorganic N isotope
192 analyses were performed with specific bacterial strains *Pseudomonas aureofaciens* for NO_3^- and
193 *Stenotrophomonas nitritireducens* for NO_2^- isotopes. These strains carry out denitrification with
194 N_2O as the end product, as they lack the N_2O reductase gene (Böhlke et al., 2007; Sigman et al.,
195 2001). The detailed laboratory protocol encompassing the preparation and handling of the bacterial
196 species, along with sample addition and isotope analysis is mentioned in previous publication (Deb
197 and Lewicka-Szczebak, 2024). Gas samples were transferred from the headspace to previously
198 evacuated Exetainer vials (Labco Limited, Ceredigion, UK), diluted and analyzed for isotope
199 values $\delta^{15}\text{N}$ and $\delta^{18}\text{O}$ values of N_2O using mass spectrometry (Thermo Scientific, MAT 253 Plus
200 mass spectrometer combined with GasBench and Precon) in the Laboratory of Isotope Geology
201 and Geoecology at the University of Wrocław, Poland.

202
203 **2.5. Laboratory Incubation of Groundwater Samples**

204 Laboratory incubation studies were conducted with groundwater samples from 4 selected
205 piezometers (P, abbreviated for piezometer: P-7, P-16, P-20, and P-23) with high nitrate
206 concentrations to investigate natural nitrate reduction and identify favorable conditions for
207 denitrification. A volume of 150 mL of groundwater from each piezometer was transferred into
208 sterile 250 mL flasks, with each sample prepared in four replicates along with sterile controls.
209 Sterile samples were produced by filtering the groundwater through 0.45 μm filters followed by
210 the addition of 2 mL of HgCl_2 to inhibit microbial activity. These sterile samples served as controls
211 for comparison with active treatments. The incubation flasks with groundwater samples were
212 flushed with N_2 gas for 15 minutes, with the flow rate 60–70 mL min^{-1} and 0.6 Bar, to create
213 suboxic conditions of similar O_2 content as in the studied aquifer. The final O_2 concentration in
214 the headspace was about 5%, which corresponds to the dissolved O_2 content in water of 2.1 mg L^{-1}
215 (Table 2). The pH of the samples, approximately 6.5 for each, was maintained without any
216 adjustments. Prior to incubation, a low amount of ^{15}N - NO_3^- labelled tracer was added to each
217 sample based on its initial nitrate concentration resulting in at% ^{15}N (Atom Percent ^{15}N) of
218 0.4296%–0.4700%, slightly exceeding the natural abundance (0.366%), to trace N transformation
219 pathways. The target $\delta^{15}\text{N}$ value of final NO_3^- was 200‰. A stock solution was prepared by
220 dissolving 12.1429 mg of $\text{Na}^{15}\text{NO}_3$ (99% ^{15}N) in 50 mL of water. From this, 1 mL was added to
221 samples P-7, P-16, and P-20, while 2 mL was added to P-23. 1 mL of glucose, equivalent to the
222 addition of 616 mg of C, was added as an additional carbon source after one week of incubation



223 to stimulate microbial activity and enhance denitrification. All samples were incubated in dark for
 224 three weeks at 16 °C with agitation at 90 rpm.

225

226 **Table 2: Data on GC headspace gas analyses for O₂, CO₂ and N₂O.**

227 The average values and standards deviations of 4 repeated incubation flasks are shown. The
 228 respective: dissolved O₂ concentration, N₂O production and CO₂ production were calculated
 229 taking into account the gas constant for gases dissolution in water for the incubation temperature
 230 of 16 C. For sterile samples the average data for the samplings before glucose addition (1 and 3)
 231 and after glucose addition (4+6).
 232

piezometer	sampling	day	O ₂ [%]		Dissolved O ₂ [mg L ⁻¹]		CO ₂ [ppm]		N ₂ O [ppb]		N ₂ O	CO ₂
			average	stdev	average	stdev	average	stdev	average	stdev	production μg/L/d	production mg/L/d
P7	1	2	8.5	1.5	3.5	865	225	918	189	0.66	1.82	
P16	1	2	7.6	1.2	3.2	761	184	524	311	0.38	1.60	
P20	1	2	7.3	1.6	3.0	391	48	258	179	0.18	0.82	
P23	1	2	7.9	0.7	3.3	575	50	365	178	0.26	1.21	
P7	3	7	4.3	2.3	1.8	1755	145	3316	3378	0.82	2.88	
P16	3	7	3.2	1.4	1.3	1129	234	540	561	0.13	1.85	
P20	3	7	3.8	1.4	1.6	337	156	527	547	0.13	0.55	
P23	3	7	4.4	1.2	1.8	762	129	654	257	0.16	1.25	
<i>flushing + glucose addition</i>												
P7	4	9	4.2	1.5	1.7	1340	294	393	246	0.28	2.82	
P16	4	9	4.4	1.3	1.8	781	329	1290	1157	0.92	1.65	
P20	4	9	2.6	1.1	1.1	426	399	133	85	0.10	0.90	
P23	4	9	2.4	0.9	1.0	326	283	497	374	0.36	0.69	
P7	6	14	3.9	2.2	1.6	1195	1545	5993	5657	1.49	1.96	
P16	6	14	2.9	1.4	1.2	1823	1369	46578	91114	11.58	2.99	
P20	6	14	2.4	1.2	1.0	1908	475	4459	7284	1.11	3.13	
P23	6	14	4.1	2.0	1.7	1807	774	2052	2050	0.51	2.96	
<i>Sterile samples</i>												
P7	1+3	4	4.4		3.0	1928		70		0.03	3.43	
P16	1+3	4	8.1		4.0	2160		224		0.09	3.84	
P20	1+3	4	5.5		2.6	632		0		0.00	1.12	
P23	1+3	4	6.4		3.3	1205		0		0.00	2.14	
<i>flushing + glucose addition</i>												
P7	4+6	4	3.5		2.6	1381		218		0.08	2.46	
P16	4+6	4	3.5		1.7	1299		1654		0.64	2.31	
P20	4+6	4	2.3		1.1	387		106		0.04	0.69	
P23	4+6	4	2.6		0.8	1044		517		0.20	1.86	



233
234 Headspace samples were periodically collected to measure N₂O concentration and isotope
235 signatures, providing insights into nitrate reduction and denitrification processes under anoxic
236 conditions. The samples of 25 mL of headspace gas were collected each second day into pre-
237 evacuated 12 mL Labco Exetainers (1 Bar overpressure). The sampled gas volume was replaced
238 with pure N₂ gas. The headspace samples were analysed on the gas chromatograph Shimadzu GC
239 Nexis 2030 equipped with barrier discharge ionisation detector (BID) and thermal conductivity
240 detector (TCD) for O₂, CO₂ and N₂O concentration (Bucha et al., 2025). The N₂O gas was analysed
241 for $\delta^{15}\text{N}$, $\delta^{18}\text{O}$ and $\delta^{15}\text{N}^{\text{SP}}$ (difference between $\delta^{15}\text{N}$ values between central and terminal position
242 of N in the linear N₂O molecule) using cavity ring-down spectroscopy (CRDS) by Picarro G5131-
243 i spectrometer equipped with small sample injection module (SSIM) and connected to SRI
244 autosampler (Eckhardt et al., unpublished) in Laboratory of Isotope Geology and Geoecology at
245 the University of Wrocław. The isotope analytical limit was about 300 ppb N₂O, for this ambient
246 concentration the measurement precision was better than 0.5‰ for $\delta^{15}\text{N}$ and $\delta^{18}\text{O}$ and better than
247 1‰ for $\delta^{15}\text{N}^{\text{SP}}$. Since this is a newly developed measurement technique, the controlled
248 measurements for selected sampling points were performed at Thünen Institute, Braunschweig,
249 Germany applying mass spectrometry (MS) (Thermo Scientific, 5 collector Delta V mass
250 spectrometer combined with Trace GC and Precon) (Lewicka-Szczebak et al., 2020). After
251 applying proper corrections to CRDS technique (Harris et al., 2020) and isotope normalization
252 with the same sets of standards the results between both approaches showed good repeatability
253 within up to 2‰ difference for $\delta^{15}\text{N}$ and $\delta^{18}\text{O}$ and up to 4‰ difference for $\delta^{15}\text{N}^{\text{SP}}$, which fits
254 within typical reasonable range for comparing measurements with different techniques (Mohn
255 et al., 2014). For sterile samples (with HgCl₂ addition) the CRDS technique gave erogenous results,
256 thus only MS results were accepted.

257 The N₂O isotope results were evaluated using modeling software FRAME (isotope FRactionation
258 And Mixing Evaluation) (<https://malewick.github.io/frame/>) to identify N₂O production pathways
259 and quantify N₂O reduction to N₂ (Lewicki et al., 2022).

260 Inorganic N levels in incubated samples were analyzed at the beginning, after one week of
261 incubation before glucose addition, and at the end of the experiment. Additionally, the isotopic
262 signatures of inorganic N were determined using bacterial denitrification by *Pseudomonas*
263 *aureofaciens* and *Stenotrophomonas nitritireducens*. The N₂O gas formed during this conversion,
264 representing nitrate or nitrite isotope signatures $\delta^{15}\text{N}$ and $\delta^{18}\text{O}$, was measured with mass
265 spectrometry (Thermo Scientific, MAT 253 Plus mass spectrometer combined with GasBench and
266 Precon).

267

268 **2.6. DNA extraction and qPCR analyses for the field and experimental samples**

269 For DNA extraction, the groundwater samples were filtered using sterile 0.45 μm mixed cellulose
270 esters (MCE) membrane filters. The filters were stored at $-80\text{ }^\circ\text{C}$ for subsequent analysis. DNA
271 was extracted from 250 mg of water filters using the DNeasy® PowerSoil® Pro Kit (Qiagen,
272 Germany), following the manufacturer's protocol with a modification: samples were homogenized
273 using a Precellys 24 homogenizer (Bertin Technologies, France) at 5000 rpm for 20 seconds. DNA



274 concentration and quality were assessed using a TECAN Infinite M200 spectrophotometer, and
 275 the extracted DNA was stored at -20°C for further microbial analysis.
 276 qPCR (quantitative Polymerase Chain Reaction) was used to quantify the bacterial and archaeal
 277 16S rRNA genes, as well as the abundances of genes involved in denitrification (*nirS*, *nirK*, *nosZI*,
 278 *and nosZII*), nitrification (bacterial, archaeal, and comammox (complete ammonia oxidation)
 279 *amoA*), nitrogen fixation (*nifH*) and dissimilatory nitrate reduction to ammonium (DNRA, *nrfA*).
 280 qPCR reactions were performed using a Rotor-Gene Q thermocycler (Qiagen, Germany). The 10
 281 μl reaction mixture consisted of 1 μl of extracted DNA, forward and reverse gene-specific primers,
 282 5 μl of Maxima SYBR Green Master mix reagent (Thermo Fisher Scientific, Waltham, MA, USA),
 283 and MilliQ water. Each sample was amplified in duplicate, with DNA-free negative control
 284 samples included in every run. The thermal cycling conditions and primers used are detailed in
 285 Table.3 (Espenberg et al., 2024). qPCR results were analyzed using Rotor-Gene® Q software
 286 v.2.0.2 (Qiagen) and LinRegPCR v.2020.2 (Netherlands). The number of gene copies was
 287 calculated based on standard curve ranges (Espenberg et al., 2018; Kuusemets et al., 2024) and
 288 expressed as gene copies per ml of water (copies mL^{-1}). DNA extraction and qPCR analysis were
 289 conducted in the Department of Geography at the University of Tartu, Estonia.

290
 291
 292
 293

Table 3: qPCR primer pairs and programs for targeted genes

Target gene	Primer	Primer concentration (μM)	Program	
bacterial 16S rRNA	Bact517F	0.3	95°C 30s; 60°C 45s;	x 40 cycles
	Bact1028R		72°C 45s	
archaeal 16S rRNA	Arc519F	0.3	95°C 15 s; 56°C 30 s;	x 45 cycles
	Arch910R		72°C 30 s	
<i>nirK</i>	nirK876	0.4	95°C 15 s, 58°C 30 s;	x 45 cycles
	nirK1040		72°C 30s, 80°C 30 s	
<i>nirS</i>	nirSCd3af	0.4	95°C 15 s, 55°C 30 s;	x 45 cycles
	nirSR3cd		72°C 30s, 80°C 30 s	
<i>nosZI</i>	nosZ2F	0.4	95°C 15 s, 60°C 30 s,	x 45 cycles
	nosZ2R		72°C 30 s, 80°C 30s	
<i>nosZII</i>	nosZIIF	1	95°C 30 s, 54°C 45 s,	x 45 cycles
	nosZIIR		72°C 45 s, 80°C 45 s	
bacterial <i>amoA</i>	amoA-1F	0.4	95°C 30 s, 57°C 45 s,	x 45 cycles
	amoA-2R		72°C 45 s	
archaeal <i>amoA</i>	CrenamoA 23F	0.4	95°C 30 s, 55°C 45 s,	x 45 cycles
	CrenamoA 616R		72°C 45 s	
comammox <i>amoA</i>	comamoA AF	0.6	95 °C 15 s, 55 °C 30 s,	x 40 cycles
	comamoA SR		72 °C 30 s	
<i>nrfA</i>	nrfAF2awMOD	0.6	95 °C 15 s, 56 °C 30 s,	x 45 cycles
	nrfAR1MOD		72 °C 30 s	
<i>nifHA</i>	Ueda19F	0.4	95 °C 30 s, 53 °C 45 s,	x 45 cycles
	Ueda407R		72 °C 45 s	



294

295 **3. Results**

296 **3.1. Dissolved inorganic N compounds**

297 **3.1.1. Inorganic nitrogen (NO_3^- , NO_2^- , NH_4^+) content and isotope signatures of initial field** 298 **samples**

299

300 Initial field samples were measured for inorganic N to determine NO_3^- , NO_2^- , and NH_4^+
301 concentration and identify piezometers with the highest nitrate levels, which were then selected
302 for laboratory incubation studies. While field measurements provided baseline reference
303 concentrations of NO_3^- , NO_2^- , and NH_4^+ , the laboratory incubation samples revealed significant
304 changes in these concentrations over the incubation period, highlighting N transformation
305 processes under controlled conditions.

306 Initial field samples before the start of incubation showed NO_3^- concentration from 0.2 mg N L⁻¹
307 to 89.5 mg N L⁻¹, NO_2^- concentration from 0.02 to 0.4 mg N L⁻¹ and NH_4^+ concentration from
308 0.02 to 17.95 mg N L⁻¹ (Table 1). The four samples with especially high nitrate concentration level
309 have been selected for further incubation studies (Table 1).

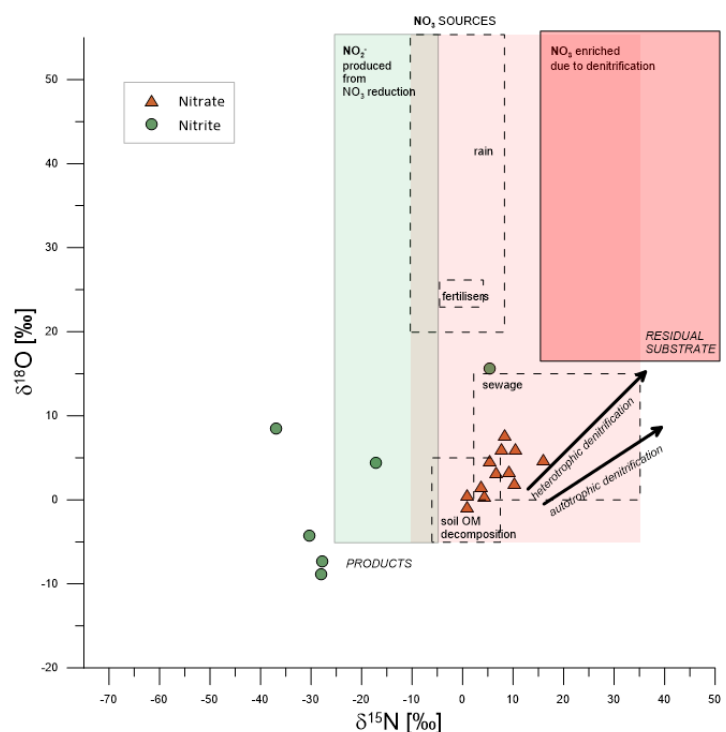
310

311 NO_3^- concentration was determined in 23 samples and NO_2^- in 22, with one sample below the
312 detection limit for NO_2^- (Table 1). But out of these 23 samples, isotope analysis of $\delta^{15}\text{N}-\text{NO}_3^-$ and
313 $\delta^{18}\text{O}_{\text{NO}_3}$ was successful on 12 samples, while $\delta^{15}\text{N}_{\text{NO}_2}$ and $\delta^{18}\text{O}_{\text{NO}_2}$ could be analyzed for 7 samples
314 only (Table 1), with the remainder samples below the detection limit for isotopic analysis. NH_4^+
315 isotopic signature was not determined because of very low concentrations below detection limit
316 for the isotope analysis. All the isotope results are presented in the following figures in the frame
317 of literature data for typical nitrate sources and denitrifying processes (Fig. 3A) and typical
318 ammonium sources and nitrifying N transformation processes (Fig. 3B) after (Deb et al., 2024).
319 Such visual presentation is applied for better identification of possible N sources and N
320 transformations.

321

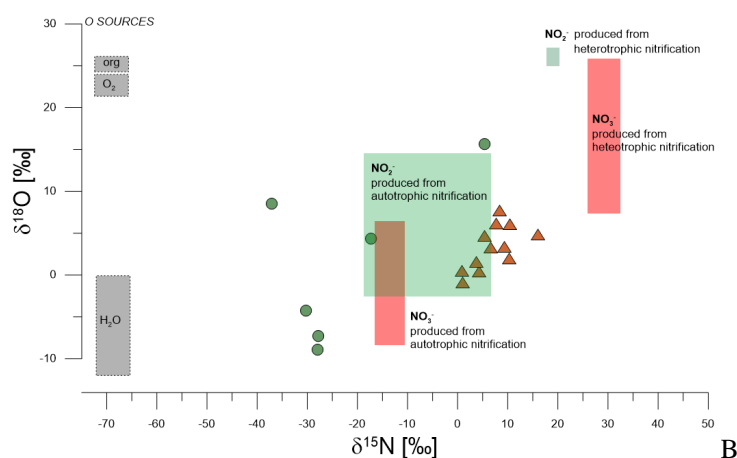
322

323



A

324
325



B

326
327

328 **Figure 3: The isotope signatures of NO_3^- (orange triangles) and NO_2^- (green circles) in field**
 329 **groundwater samples presented with the literature data for particular N sources and isotope**
 330 **effects for main N transformations, with respect to denitrification processes (A) and**
 331 **nitrification nitrite and nitrate sources (B). The literature data shown as boxes after (Deb et al.,**
 332 **2024). In (A) NO_3^- sources (pink rectangles) include rain, fertilizers, sewage, and soil organic**
 333 **matter, while products (green rectangle) include NO_2^- , formed during NO_3^- reduction. Residual**
 334 **NO_3^- enriched through denitrification is represented in the red rectangle. Arrows depict typical**



335 isotope effect associated with autotrophic and heterotrophic processes. In (B) isotopic
336 characteristics of NO_2^- (green rectangles) and NO_3^- (red rectangles) originating from autotrophic
337 and heterotrophic nitrification is shown. Grey rectangles illustrate possible oxygen sources (O_2 and
338 H_2O) used during nitrifying oxidation processes.

339

340 **3.1.2 Inorganic nitrogen (NO_3^- , NO_2^- , NH_4^+) content and isotope signatures during** 341 **incubation**

342 During the first phase (before glucose addition), NO_3^- concentrations decreased significantly
343 across all samples (decrease of 14 to 33 mg L^{-1} N was noted, Fig.4A). Concurrently, NO_2^-
344 concentrations increased significantly reaching around 3.7 to 13.5 mg L^{-1} N, Fig.4A). In the second
345 phase (after glucose addition), NO_3^- concentrations continue to decrease in all samples (further
346 decrease of 6.2 to 47.6 mg L^{-1} N compared to day 7 sample, Fig.4A), while NO_2^- levels further
347 increase for most samples reaching 4.7 to 13.5 mg L^{-1} N. NH_4^+ concentrations were very low from
348 0 to 0.2 mg L^{-1} N) and remained largely unchanged throughout the incubation period.

349 Further, the isotopic signatures of nitrate ($\delta^{15}\text{N}_{\text{NO}_3}$ and $\delta^{18}\text{O}_{\text{NO}_3}$) and nitrite ($\delta^{15}\text{N}_{\text{NO}_2}$ and $\delta^{18}\text{O}_{\text{NO}_2}$)
350 were analysed in water samples during laboratory incubation (Fig 4B). $\delta^{15}\text{N}_{\text{NO}_3}$ shows much higher
351 values when compared to initial field samples (Fig. 3) due to low addition of ^{15}N - NO_3^- tracer. The
352 preparation of tracer solution and amount of tracer addition was calculated to attain ca. 100-200
353 ‰ as the final $\delta^{15}\text{N}_{\text{NO}_3}$ value. However, due to different initial NO_3^- concentrations and precision
354 of the low amount tracer addition, our final $\delta^{15}\text{N}_{\text{NO}_3}$ after tracer addition is variable for each of the
355 four incubated samples from approximately 100‰ for P-23 to over 300‰ for P-20 (Fig. 4B).
356 However, these different final values have been taken into account by all calculations and
357 modelling, so that the differences did not impact the data interpretation. All calculations were
358 applied individually for each incubated water sample and individual $\delta^{15}\text{N}_{\text{NO}_3}$ values have been
359 accepted as the incubation starting point for each of the four water samples. $\delta^{15}\text{N}_{\text{NO}_3}$ and $\delta^{18}\text{O}_{\text{NO}_3}$
360 increase significantly during the first phase of incubation and remain quite stable during the second
361 incubation phase across all samples. $\delta^{15}\text{N}_{\text{NO}_2}$ shows slight variability across all samples, with values
362 ranging from approximately -50‰ to 0‰, hence much lower than the respective $\delta^{15}\text{N}_{\text{NO}_3}$ values.
363 $\delta^{18}\text{O}_{\text{NO}_2}$ shows very dynamic variations without very consistent trends, reflecting the complexity
364 of microbial and environmental interactions affecting nitrite transformation. Interestingly, there is
365 very clear pattern for P-7, P-16 and P-20 with significant $\delta^{18}\text{O}_{\text{NO}_2}$ enrichment for the 2nd sampling
366 (7 days) and further depletion for the 3rd sampling (14 days) (Fig. 4B).

367 In the sterile treatment the NO_3^- reduction is even faster than in other samples, while the isotope
368 signatures are very stable showing very minor isotope enrichment. NO_2^- concentrations are very
369 low not exceeding 0.3 mg N L^{-1} . NH_4^+ concentrations increase during the incubation reaching up
370 to 4 mg N L^{-1} , which is much higher than observed for non-sterile samples.

371

372

373

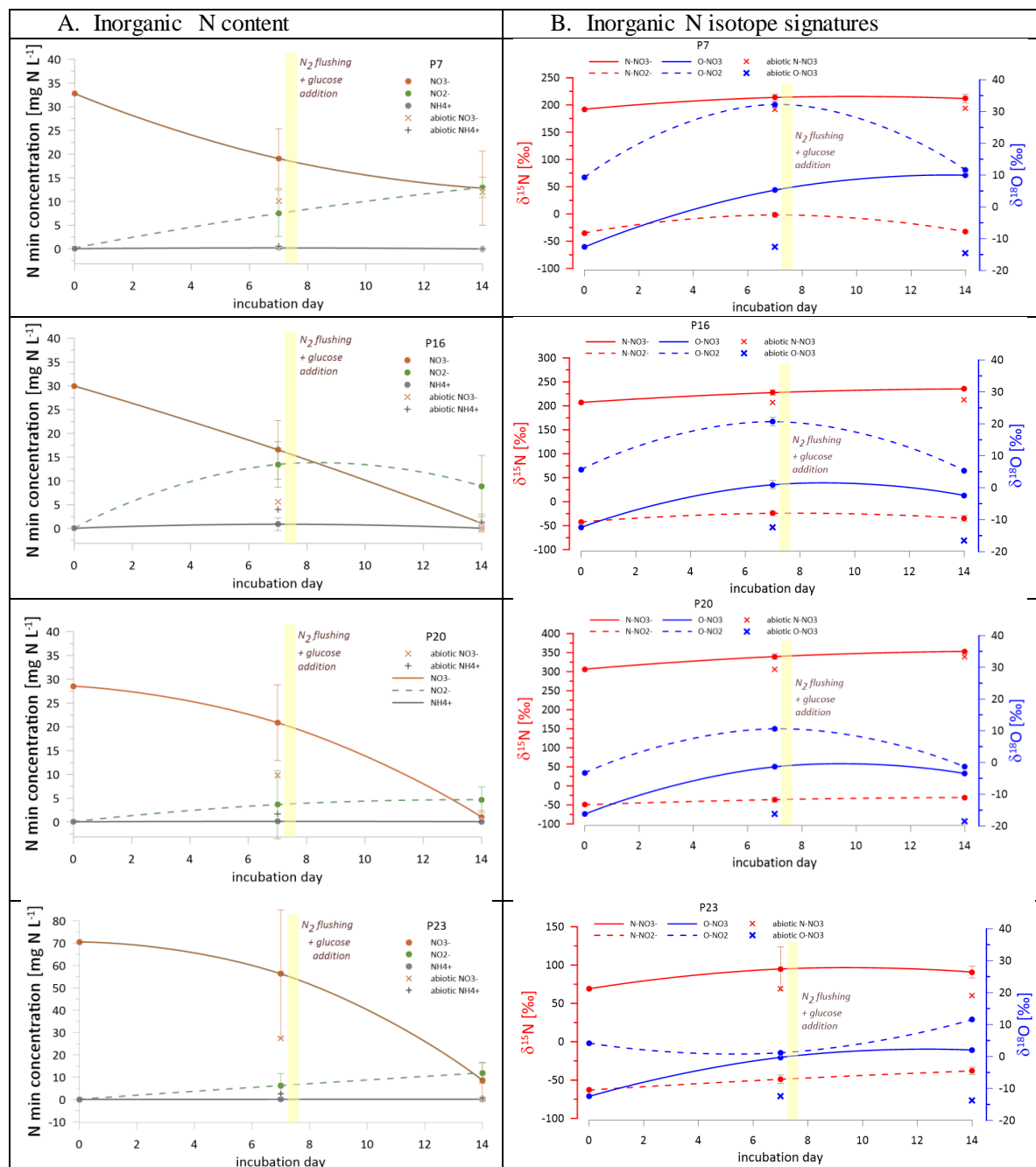
374

375

376



377



378
 379
 380
 381

Figure 4. Content of inorganic nitrogen forms (orange line: NO₃⁻, green line: NO₂⁻, grey line: NH₄⁺) and their isotopic signatures (δ¹⁵N and δ¹⁸O) during laboratory incubation. The graphs in A show concentrations variation in time and graphs in B depict changes in δ¹⁵N (red



382 lines) and $\delta^{18}\text{O}$ (blue lines) values over time for nitrate (solid line) and nitrite (dashed line) in
383 different samples (P, abbreviated for piezometer: P-7, P-16, P-20, and P-23), illustrating dynamic
384 isotopic variations influenced by microbial processes. Sterile samples are shown as the individual
385 points on the graphs (for NO_3^- and NH_4^+ contents, while NO_2^- was very low for all the sterile
386 samples, and is not shown).

387

388

389

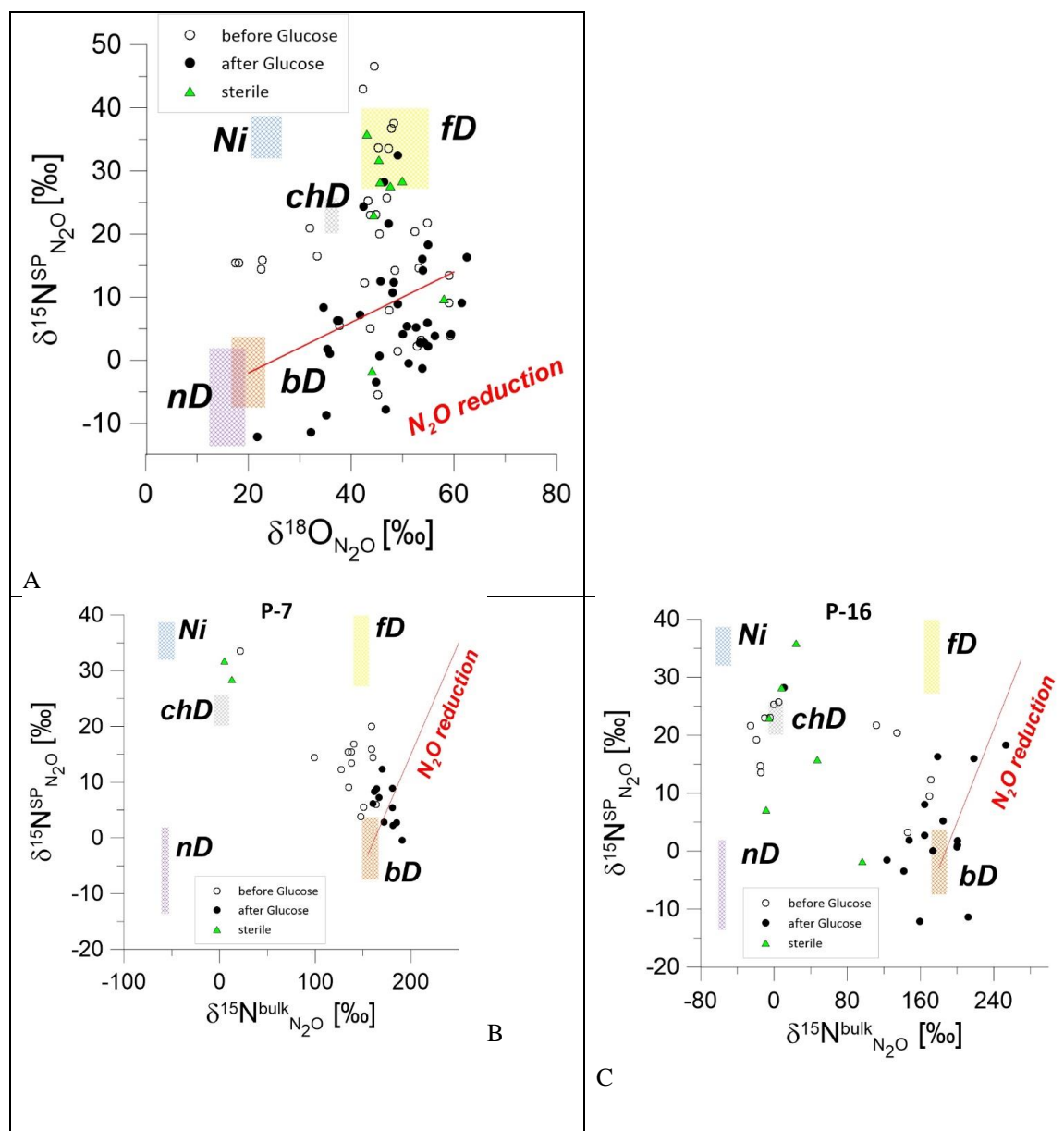
390 **3.2. Gas headspace sample analysis**

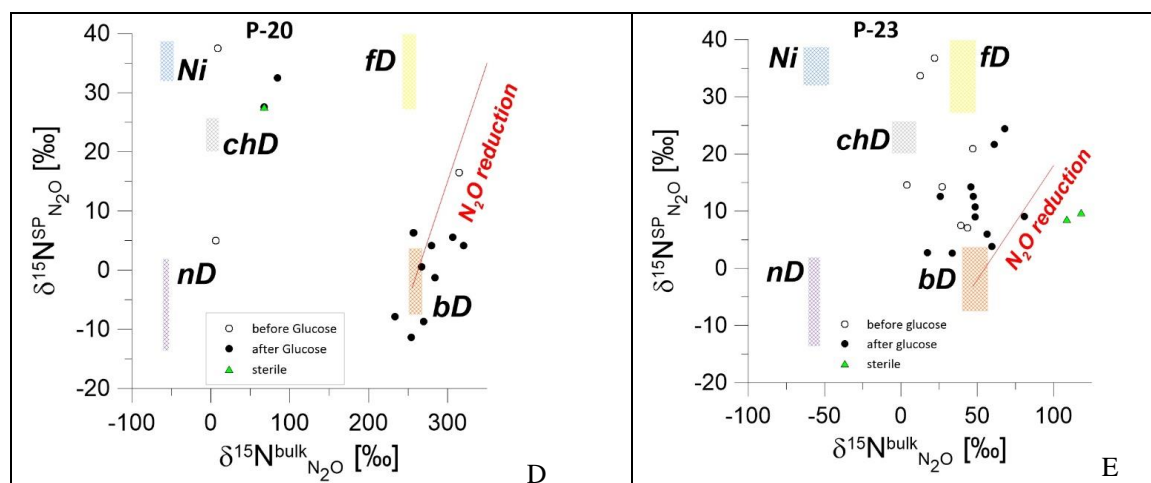
391 For almost all samplings significant N_2O and CO_2 fluxes were observed during the incubation. The
392 gases were accumulated in the headspace until day 7 of the incubation (phase 1: day 1 – day 7),
393 then after flushing the accumulation was started again for next 7 days (phase 2: day 8 – day 14).
394 Table 2 shows results of headspace gas analyses for the second and last day of the accumulation,
395 for each incubation phase, before and after glucose addition. The CO_2 production varies from 0.7
396 to $3.1 \text{ mg L}^{-1} \text{ day}^{-1}$ with similar flux range for both phases. The N_2O production varies from 0.1 to
397 $11.6 \text{ } \mu\text{g L}^{-1} \text{ day}^{-1}$ with significantly higher fluxes for the second incubation phase, with one
398 extremely high outlier.

399 Sterile samples show CO_2 production in the comparable amount to unsterile treatments, and much
400 lower N_2O production, however still significant for some points, especially for the second
401 incubation phase after glucose addition (Table 2).

402 Figure 5 shows the isotopic signatures ($\delta^{15}\text{N}^{\text{SP}}$, $\delta^{18}\text{O}$, $\delta^{15}\text{N}$) of N_2O in headspace samples from
403 laboratory incubation before and after glucose addition together with the main N_2O production
404 pathways and typical N_2O reduction line summarized after literature data (Yu et al., 2020). The
405 isotope characteristics for the main N_2O production pathways: bacterial and fungal denitrification
406 (bD and fD), nitrifier denitrification (nD), nitrification (Ni) and chemodenitrification (chD) are
407 shown for the particular substrate isotopic signatures of the actual case study: $\delta^{18}\text{O}_{\text{H}_2\text{O}}$ of -9.0‰
408 (mean common value for all water samples) and respective $\delta^{15}\text{N}_{\text{NO}_3}$, separately for each sampling
409 point (respective values in Table 1).

410





411

412

413

414

415

416

417

418

419

420

421

422

423

424

425

426

427

428

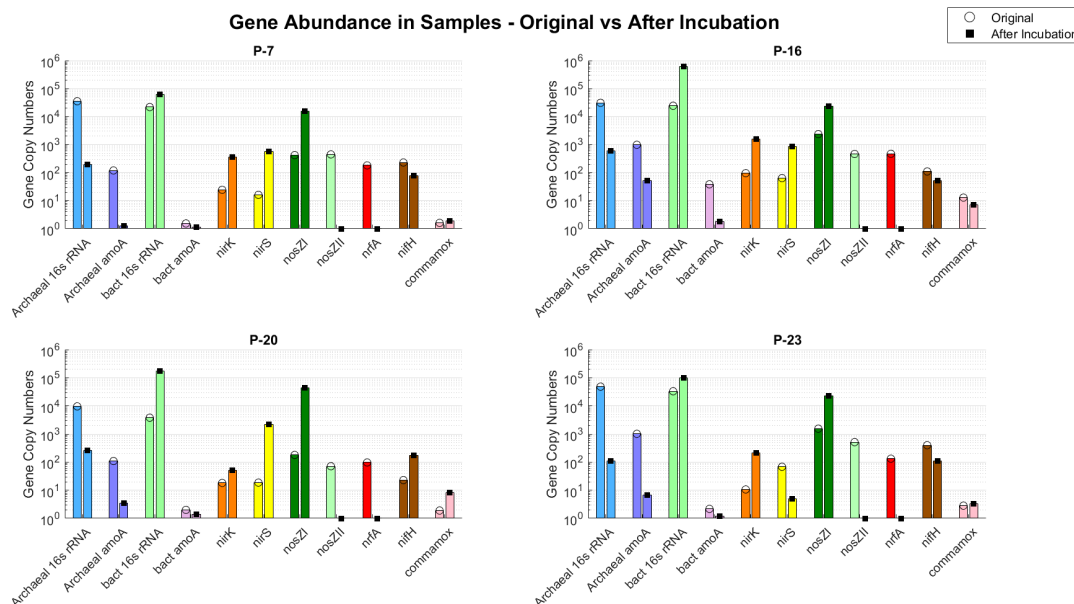
429

430

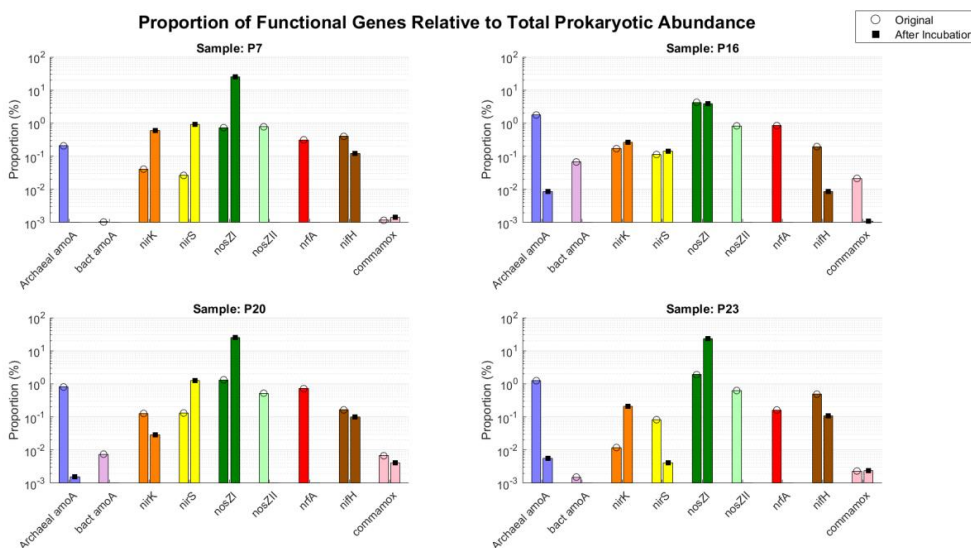
Figure 5 : Isotopic signatures ($\delta^{15}\text{N}^{\text{SP}}_{\text{N}_2\text{O}}$, $\delta^{18}\text{O}_{\text{N}_2\text{O}}$ and $\delta^{15}\text{N}_{\text{N}_2\text{O}}$) highlighting N_2O dynamics and microbial nitrogen transformation pathways during laboratory incubation for groundwater samples (P, abbreviated for piezometer: P-7, P-16, P-20, and P-23). Empty circles represent the first incubation phase, filled circles – the second incubation phase after glucose addition and green triangles show sterile samples. Clustering reflects a shift from mixed nitrification and denitrification before glucose addition to bacterial denitrification dominance after glucose addition. Panel A presents $\delta^{15}\text{N}^{\text{SP}}-\delta^{18}\text{O}$ map for all samples, since the source processes are common for all samples, panels B-E present $\delta^{15}\text{N}^{\text{SP}}-\delta^{15}\text{N}$ maps individually plotted for each piezometers, because depending on the particular ^{15}N content for each piezometer the mixing endmembers isotopic signatures (bD and fD) differ. Each plot shows isotopic values before glucose addition (white circles) and after glucose addition (black circles), reflecting microbial processes like bacterial denitrification (bD), autotrophic nitrification (Ni), nitrifier denitrification (nD), and fungal denitrification (fD), with N_2O reduction along the red line.

3.3 Gene abundance and proportion analyses

The gene abundance graph (Fig 6A) illustrates the quantification of key nitrogen cycle genes while the proportions of functional genes relative to total prokaryotic abundance are shown in Fig 6B for groundwater samples (P-7, P-16, P-20, and P-23) before and after incubation.



431
 432 **Figure 6 (A): Comparison of gene abundance in groundwater samples before and after**
 433 **incubation**



434
 435 **Figure 6 (B): Functional Gene Proportions Pre- and Post-Incubation**

436 The graphs (Fig. 6A and Fig. 6B) illustrate the abundance and proportions of key nitrogen cycle
 437 genes in groundwater samples (P-7, P-16, P-20, and P-23) before and after incubation. Figure 6A
 438 shows the relative abundance of genes involved in nitrification (archaeal *amoA*, bacterial *amoA*),
 439 denitrification (*nirK*, *nirS*, *nosZI*, *nosZII*), nitrogen fixation (*nifH*), and DNRA (*nrfA*), as well as
 440 complete nitrification (*commamox*) alongside microbial population markers (archaeal and



441 bacterial 16s rRNA). Figure 6B presents the proportions of these functional genes relative to total
442 prokaryotic abundance, highlighting their contributions to the microbial community structure.

443

444 **4 Discussion**

445 **4.1 Initial groundwater samples – N transformations occurring in field conditions**

446 For identification of possible N-transformations occurring naturally in the aquifer the isotope
447 signatures of inorganic N (NO_3^- and NO_2^-) were compared with the literature data on
448 denitrification (Fig. 3A) and nitrification (Fig. 3B).

449 Figure. 3A illustrates the isotopic composition ($\delta^{15}\text{N}$ and $\delta^{18}\text{O}$) of NO_3^- in groundwater samples,
450 highlighting both the sources of nitrate and the processes that transformed it during the residence
451 time in the aquifer. Samples in the pink-shaded zone reflect NO_3^- contributions from sources such
452 as fertilizers, sewage, and soil organic matter decomposition, with minimal microbial
453 transformation. Samples with enriched $\delta^{15}\text{N}$ and $\delta^{18}\text{O}$ values, located in the red-shaded "Residual
454 Substrate" zone, indicate advanced denitrification, where residual nitrate is enriched in ^{15}N and
455 ^{18}O due to preferential reduction of light isotopes. The green-shaded area represents NO_2^-
456 produced from NO_3^- reduction during partial denitrification, an intermediate step in denitrification.
457 The isotopic patterns in the graph also differentiate between autotrophic and heterotrophic
458 denitrification. Samples aligning with autotrophic denitrification indicate the reduction of NO_3^-
459 coupled with the oxidation of inorganic compounds like sulfur or hydrogen, resulting in a slower
460 rate of isotopic fractionation and less pronounced enrichment in $\delta^{15}\text{N}$ and $\delta^{18}\text{O}$ (Cui et al., 2019;
461 Hu et al., 2024). In contrast, samples reflecting heterotrophic denitrification show rapid isotopic
462 fractionation due to the use of organic carbon as the electron donor, leading to greater enrichment
463 of $\delta^{15}\text{N}$ and $\delta^{18}\text{O}$ in the residual nitrate (after (Deb et al., 2024)).

464 Our NO_3^- samples (orange triangles, Fig. 3A) are located in the area typical for NO_3^- originating
465 from organic matter decomposition and of sewage origin. The precise knowledge of the $\delta^{15}\text{N}$
466 signature of the potential N substrates, i.e. of DON and waste waters, could further confirm the
467 dominant source of the samples (Boumaiza et al., 2024). The nitrate samples present a clear
468 correlation between $\delta^{18}\text{O}$ and $\delta^{15}\text{N}$ values, typical for isotope enrichment due to heterotrophic
469 denitrification leading to ^{18}O and ^{15}N enriched of the residual NO_3^- . However, this enrichment is
470 relatively low and the samples do not show typically high δ values (Fig. 3A). This indicates that
471 the nitrate pool might be constantly renewed with fresh substrate of low δ values.

472 Our NO_2^- samples (green circles, Fig. 3A), are mostly shifted towards lower $\delta^{15}\text{N}$ values, with the
473 expected isotope effect typical for denitrification NO_3^- reduction to NO_2^- , with isotopically
474 depleted NO_2^- due to the preferential reduction of light isotopes (^{14}N and ^{16}O). $\delta^{18}\text{O}_{\text{NO}_2}$ values are
475 similar or lower than the respective NO_3^- source, which may indicate additional incorporation of
476 water into the formed NO_2^- .

477 Figure .3B illustrates the isotopic composition of nitrate (NO_3^-) and nitrite (NO_2^-) in groundwater
478 samples in regard to possible nitrification processes. Autotrophic nitrification, with NO_3^- produced
479 from NH_4^+ or organic nitrogen, is characterized by lower $\delta^{15}\text{N}$ and $\delta^{18}\text{O}$ values, while heterotrophic
480 nitrification contributes to NO_3^- and NO_2^- production with distinct isotopic enrichment from
481 organic nitrogen compounds. Our NO_3^- samples are located between values typical for NO_3^-



482 production from autotrophic and heterotrophic nitrification, the observed correlation might be a
483 mixing between these two NO_3^- origins. However, from the NO_2^- samples only two points indicate
484 typical values for autotrophic nitrification, whereas others show much lower $\delta^{15}\text{N}$ values (Fig. 3B).
485 Both graphs show the potentially occurring processes, it is important to review them jointly with
486 the basic aquifer information and further microbial analyses and incubation studies. The
487 physicochemical parameters for our aquifer present redox conditions theoretically allowing for
488 occurrence of both denitrification and nitrification processes. Oxygen concentrations in the range
489 of less than 1 and up to $2 \text{ mg O}_2 \text{ L}^{-1}$ are regarded as the boundary between nitrate-reducing and
490 non-nitrate-reducing conditions in groundwater (Wolters et al., 2022). Hence, the range of
491 dissolved oxygen content observed for the aquifer under study of $2.2 - 4.3 \text{ mg O}_2 \text{ L}^{-1}$ is slightly
492 higher, and denitrifying processes might be suppressed. The redox potential of our aquifer of 213-
493 345 mV lies also on the edge of typical denitrifying conditions from 10 to 300 mV (Brettar et al.,
494 2002). This suggests that reduction processes might occur but might be also accompanied by
495 oxidation processes. Consequently, both conclusions drawn from the Fig. 3A and 3B might be
496 simultaneously true. Whereas NO_3^- is being denitrified it might be simultaneously produced both
497 in autotrophic and heterotrophic nitrification, which is supported by only small NO_3^- enrichment.
498 Groundwater samples of dominant denitrification show much higher NO_3^- isotope signatures
499 (Clague et al., 2019). Similarly, NO_2^- isotopic signature shows most probably a mixture of NO_3^-
500 reduction and formation due to nitrification, in various proportions for different samples. There is
501 one sample of the highest $\delta^{18}\text{O}_{\text{NO}_2}$ and $\delta^{15}\text{N}_{\text{NO}_2}$ (Fig. 3B). This is the P-L2-1 piezometer located
502 closest to the lagune of yeast sewage storage, the sample of the highest NH_4^+ content (Table 1). In
503 this sample NO_2^- must originate mostly from autotrophic nitrification from ammonium oxidation,
504 as it can be concluded from Fig. 3B.

505 The conclusion of active nitrification processes is reinforced with the gene abundances observed
506 in field samples, before incubation, Fig. 6, where the majority of gene copy numbers represent
507 archaeal *amoA*, while denitrification genes occurrence is very low. Hence, we rather have intensive
508 nitrate production by nitrification processes (Fig. 3B).

509 To further figure out which potential N transformations are active in the aquifer we performed the
510 laboratory incubations in controlled conditions of selected water samples.

511

512 **4.2 Active N transformation processes during incubation**

513 **4.2.1. Inorganic N analyses**

514 The dynamic variations in inorganic N concentration and isotopic evolution of NO_3^- and NO_2^-
515 during the laboratory incubation experiments (Fig. 4) across all incubated samples (P-7, P-16, P-
516 20, and P-23) reflects active microbial transformations during the incubation period. Prior to
517 glucose addition, the observed decrease in NO_3^- concentration, coupled with a parallel increase in
518 $\delta^{18}\text{O}_{\text{NO}_3}$ and $\delta^{15}\text{N}_{\text{NO}_3}$ (Fig.4), suggests intensive denitrification with preferential reduction of light
519 isotopes resulting in enrichment of the residual nitrate. The apparent isotope effect, i.e. the
520 difference between the initial and final (after 7 days) NO_3^- isotope signature is from 20 to 33‰ for
521 $\delta^{15}\text{N}_{\text{NO}_3}$ and from 12 to 18‰ for $\delta^{18}\text{O}_{\text{NO}_3}$ giving O/N ratio from 0.45 to 0.83, which is typical slope
522 for heterotrophic denitrification (from 0.48 to 0.88) (Boumaiza et al., 2024; Clague et al., 2019).



523 During this first phase the NO_2^- concentration clearly increase from near 0 to a few $\text{mg NO}_2^- \text{ L}^{-1}$
 524 and $\delta^{15}\text{N}_{\text{NO}_2}$ values show slight increase (Fig.4). This shows that the elevated $\delta^{15}\text{N}_{\text{NO}_3}$ (due to low-
 525 level labeling) is partially transferred to the NO_2^- pool. However, the low magnitude of this
 526 increase is rather surprising, i.e., the $\delta^{15}\text{N}_{\text{NO}_2}$ do not approach the high values of NO_3^- , but increase
 527 only slightly. This indicates that the formed nitrite must partially originate from another ^{15}N -
 528 depleted pool (unlabelled). Based on the observed $\delta^{15}\text{N}_{\text{NO}_3,0}$ (initial value, day 0) and change in
 529 $\delta^{15}\text{N}_{\text{NO}_2}$ values (between day 0 and day 7 of the incubation) we can calculate the maximal
 530 contribution of NO_2^- -originating from NO_3^- -reduction (NAR) in this new-formed NO_2^- applying the
 531 isotope mass balance (Eq.1). These calculations are simplified by neglecting any isotope
 532 fractionation of the NO_2^- pool.

$$533 \quad \text{NAR} = \frac{\delta^{15}\text{N}_{\text{NO}_2-7} - \delta^{15}\text{N}_{\text{NO}_2-0}}{\delta^{15}\text{N}_{\text{NO}_3-0}} \quad (\text{Eq.1})$$

534

535 **Table 4: Inputs and results of the mass balance calculations for determining the contribution**
 536 **of nitrate reduction (NAR) in the nitrite pool** with Eq.1: $\Delta\delta^{15}\text{N}_{\text{NO}_2}$ is the change of nitrite N
 537 isotope signature between day 0 and day 7, $\delta^{15}\text{N}_{\text{NO}_3,0}$ - initial N isotope signature of nitrate, Δ
 538 $[\text{NO}_2^-]$ is the change of nitrite concentration between day 0 and day 7, mg/L NAR is the amount
 539 of produced nitrite originating from NAR, $\Delta [\text{NO}_3^-]$ is the nitrate consumption between day 0 and
 540 day 7.

541

Piezometer	$\Delta\delta^{15}\text{N}_{\text{NO}_2}$	$\delta^{15}\text{N}_{\text{NO}_3,0}$	NAR [%]	$\Delta [\text{NO}_2^-] \text{ mg N L}^{-1}$	mg/L NAR	$\Delta [\text{NO}_3^-] \text{ mg N L}^{-1}$
P-7	33.1	192.2	17.2	7.3	1.3	-13.7
P-16	18.1	207.1	8.7	13.4	1.2	-23.0
P-20	13.4	306.5	4.4	3.6	0.2	-17.2
P-23	14.1	69.0	20.4	6.1	1.2	-33.2

542

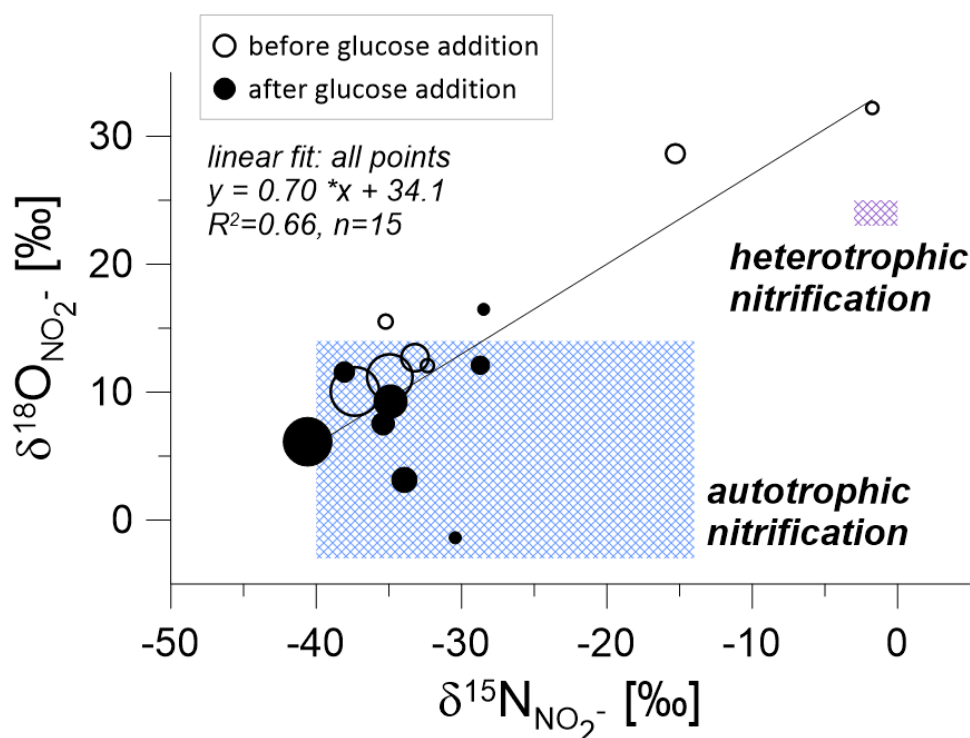
543 The calculation results (Table 4) indicate that from 0.2 up to 1.3 $\text{mg N-NO}_2^- \text{ L}^{-1}$ originates from
 544 NAR, which is low amount when compared to the magnitude of N-NO_3^- consumption of 13.7 to
 545 33.2 mg L^{-1} (Table 4). This agrees with the fact that NO_2^- is a very reactive and short living
 546 compound and as denitrification intermediate it instantaneously undergo further reduction
 547 (Lewicka-Szczebak et al., 2021). But interestingly, the large majority of N-NO_2^- (80 to 95 %)
 548 originates from other transformations than NO_3^- reduction. Since the NH_4^+ contents are very low
 549 in all the samples, this unlabelled N source for NO_2^- production must originate from dissolved
 550 organic N (DON). This pathway is very plausible since the samples show high DON contents from
 551 31 to 92 mg N L^{-1} (Table 2). For most samples, NO_2^- show significant increase in $\delta^{18}\text{O}_{\text{NO}_2}$ values
 552 in the first phase (between day 0 and day 7), indicating that the major source of O must be
 553 molecular O_2 with characteristic high $\delta^{18}\text{O}_{\text{O}_2}$ of +23.5‰ (Moore et al., 2006). Since the incubations
 554 applied suboxic atmosphere (up to 5% in the headspace and 2.1 mg of dissolved oxygen (Table 2),
 555 this low amounts of oxygen must have been used or the oxygen must had been fixed before in
 556 other compounds, like organic matter, and further used for oxidation processes. Only for P-23 the
 557 $\delta^{18}\text{O}_{\text{NO}_2}$ value stays stable, this sample shows most intensive NO_3^- reduction due to denitrification



558 and most probably the potential increase was masked with O-atoms exchange between water and
559 denitrification intermediates (Lewicka-Szczebak et al., 2016).
560 In the second phase of the incubation, after glucose addition, further NO_3^- reduction was observed
561 in all samples (Fig. 4A). However, despite this observed reduction, δ value stay quite stable, with
562 much less isotope enrichment between day 7 and 14 of the incubation, when compared to the day
563 0 - day 7 enrichment, both for $\delta^{15}\text{N}$ and $\delta^{18}\text{O}$ (Fig. 4B). Hence, we do not observe here the typical
564 isotope enrichment characteristic for denitrification processes (Boumaiza et al., 2024). The
565 occurrence of intensive denitrification during the second incubation phase can be clearly proved
566 with N_2O data, which show high ^{15}N content, and $\delta^{15}\text{N}^{\text{SP}}$ and $\delta^{18}\text{O}$ values typical for bacterial
567 denitrification (Fig. 5). Also analysed gene abundances clearly indicate intensification of
568 denitrification genes during the incubation (Fig. 6). But despite active denitrification process, the
569 typical isotope enrichment is not observed. This might possibly indicate significant additional
570 contribution of other process of nitrate reduction. Chemodenitrification can be considered, since
571 this process is associated with no kinetic isotope effects for either $\delta^{15}\text{N}$ or $\delta^{18}\text{O}$ in the residual
572 NO_3^- pool (X. Wang et al., 2022). This assumption can be reinforced with the sterile samples data,
573 where nitrate pool is also largely reduced (Fig. 4A) without any isotope effects (Fig. 4B). This
574 indicates that the conditions in the studied groundwaters support chemodenitrification.
575 Simultaneously, $\delta^{15}\text{N}_{\text{NO}_2^-}$ mostly go down or increase only slightly, indicating that the
576 transformations of unlabelled N source are getting even more active than in the first incubation
577 phase and there is nearly no detectable contribution of NO_2^- from NO_3^- reduction. However, the
578 labelled ^{15}N is present in the further denitrification product – N_2O , hence it must have been
579 transformed through NO_2^- as the first denitrification intermediate. This shows that this conversion
580 takes place very rapidly, maybe even in the same microbial cell and NO_2^- must be nearly
581 completely converted to further denitrification products. Importantly, the common pool of NO_2^- ,
582 which do not show ^{15}N enrichment, is mostly not converted to N_2O . This is proven by the fact that
583 $\delta^{15}\text{N}_{\text{N}_2\text{O}}$ values are very close to $\delta^{15}\text{N}_{\text{NO}_3^-}$, but much higher than $\delta^{15}\text{N}_{\text{NO}_2^-}$ during the second
584 incubation phase. Hence, the NO_2^- newly formed in nitrification processes is not further reduced
585 to N_2O but is most probably rather further oxidised to NO_3^- . Since this process would add ^{15}N
586 depleted NO_3^- this can mask the ^{15}N enrichment due to denitrification. In this second incubation
587 phase, O isotope signatures of NO_2^- and NO_3^- mostly move towards each other, which indicates
588 probably intensive reversible reactions of reduction and oxidation between these two compounds,
589 which facilitates O-atoms exchange with water. This agrees with the recent findings by (Zheng et
590 al., 2023) who indicated tighter cycling between these both compounds with particular importance
591 of NO_2^- re-oxidation processes. The inconsistencies found in our data for ^{15}N content in NO_3^- ,
592 NO_2^- and N_2O pool reinforces the assumption of separate NO_2^- pools for particular N
593 transformation pathways (Müller et al., 2014; Rütting and Müller, 2008; Zhang et al., 2023).
594 Although most of these previous studies apply for soils, it is apparently also true for groundwater
595 N transformations.
596 A closer look on the isotopic analysis of nitrite (NO_2^-) in the groundwater incubation study (Fig.
597 7) reveals that the highest nitrite concentrations are characterised by the lowest isotope signatures.



598 We observe a statistically significant correlation between O and N isotopic signatures of NO_2^- .
599 Theoretically, this could be the mixing line with the ^{15}N labelled values originating from labelled
600 NO_3^- , reduction, but this NO_3^- , shows low $\delta^{18}\text{O}$ values in the range from -16 to +10‰. Hence, this
601 rather shows mixing of the different origins of unlabelled NO_2^- , which is in great majority (as
602 shown above and in Table 4), potentially originating from both autotrophic and heterotrophic
603 nitrification processes.
604
605



606 **Figure 7: Isotopic Signatures of Nitrite (NO_2^-) during laboratory Incubation: first phase,**
607 **before glucose addition: empty circles, second phase, after glucose addition: filled circles.**
608 The points size is proportional to nitrite concentration. The shaded regions correspond to isotopic
609 ranges associated with autotrophic and heterotrophic nitrification (after (Deb et al., 2024)),
610 illustrating a shift in processes following glucose addition.
611

612
613 Before the addition of glucose, the isotopic signatures (empty circles) predominantly cluster within
614 the autotrophic nitrification zone, indicating that autotrophic bacteria initially dominated nitrite
615 production by converting ammonia to nitrite using CO_2 . Autotrophic bacteria, such as
616 *Nitrosomonas europaea* convert ammonia (NH_3) to nitrite (NO_2^-) as an energy-generating process
617 (Deb et al., 2024). During this process, CO_2 serves as the sole carbon source for these bacteria,
618 assimilated into their biomass to support cellular growth, independent of the chemical reaction
619 used for energy generation (Hommes et al., 2003). In the groundwater samples, CO_2 likely



620 originated from the decomposition of organic matter in the yeast sewage (Section 2.1) or from the
621 carbonate system naturally present in groundwater (Section 3.1.1).

622 The application of yeast-based sewage as fertilizer in the agricultural site likely introduced organic
623 nitrogen into the groundwater, which undergoes microbial decomposition to release ammonium
624 (NH_4^+) through the mineralization of proteins and amino acids (Watanabe et al., 2023). However,
625 NH_4^+ was not detected in the groundwater samples (Table 1), indicating its rapid transformation
626 within the nitrogen cycle. The absence of NH_4^+ can be attributed to its immediate consumption
627 through autotrophic nitrification, where ammonia is oxidized to NO_2^- and NO_3^- . The clustering of
628 isotopic data within the autotrophic nitrification zone in Fig. 7 before glucose addition supports
629 this process, highlighting ammonia oxidation as a dominant pathway. Additionally, microbial
630 assimilation likely contributed to NH_4^+ exhaustion, as microbes utilized it for biomass synthesis.
631 This is not the case for sterile samples, where we observe slight accumulation of NH_4^+ .

632 Following glucose addition, the isotopic signatures (filled circles) become more dispersed, with
633 several data points shifting towards the heterotrophic nitrification zone. This shift suggests that
634 glucose addition stimulated heterotrophic bacteria, altering nitrite production pathways. While
635 autotrophic nitrification likely continued, the spread in isotopic values indicates that heterotrophic
636 nitrifiers also contributed to nitrite production, likely utilizing organic nitrogen compounds,
637 supporting a transition from predominantly autotrophic to mixed nitrification processes. Together,
638 these findings demonstrate the rapid transformation of NH_4^+ from yeast-based fertilizers into
639 intermediate nitrogen compounds, driving nitrification and subsequent nitrogen cycling processes
640 in groundwater.

641

642 **4.2.2 Headspace N_2O analyses and FRAME isotope model**

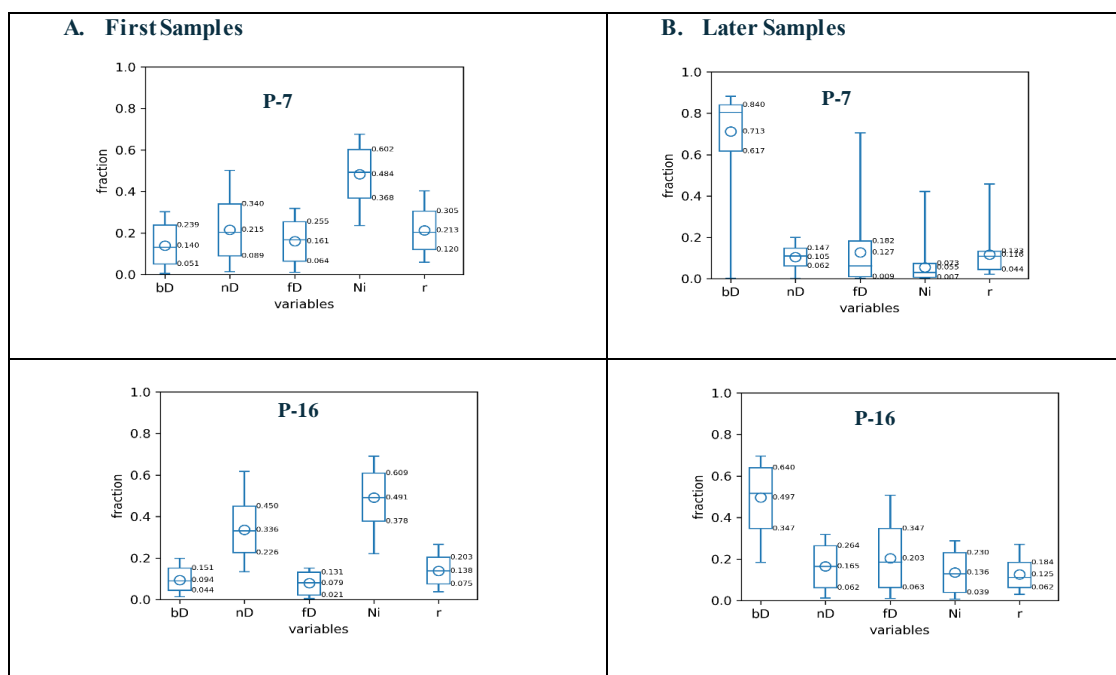
643 Figure 5 illustrates the isotopic signatures ($\delta^{15}\text{N}^{\text{SP}}_{\text{N}_2\text{O}}$, $\delta^{18}\text{O}_{\text{N}_2\text{O}}$ and $\delta^{15}\text{N}_{\text{N}_2\text{O}}$) of N_2O in headspace
644 samples collected during laboratory incubation with the relevant microbial N transformation
645 pathways presented based on the literature data (Yu et al., 2020) and taking into account the actual
646 measured isotopic signatures of sources applied in this case study ($\delta^{18}\text{O}_{\text{H}_2\text{O}}$, $\delta^{15}\text{N}_{\text{NO}_3^-}$). Before
647 glucose addition (white dots), the isotopic signatures indicate mixing between nitrification and
648 denitrification processes (Fig. 5A). In P-7, before glucose addition, isotopic data clustered near the
649 nitrifier denitrification (nD) zone, highlighting ammonia oxidation and partial N_2O reduction. In
650 P-16, isotope signatures widely distributed between nitrifier and bacterial denitrification zones,
651 suggesting overlapping processes. In P-20 and P-23, clustering near the bacterial denitrification
652 (bD) zone reflected nitrate reduction as the dominant pathway with minimal N_2O reduction.

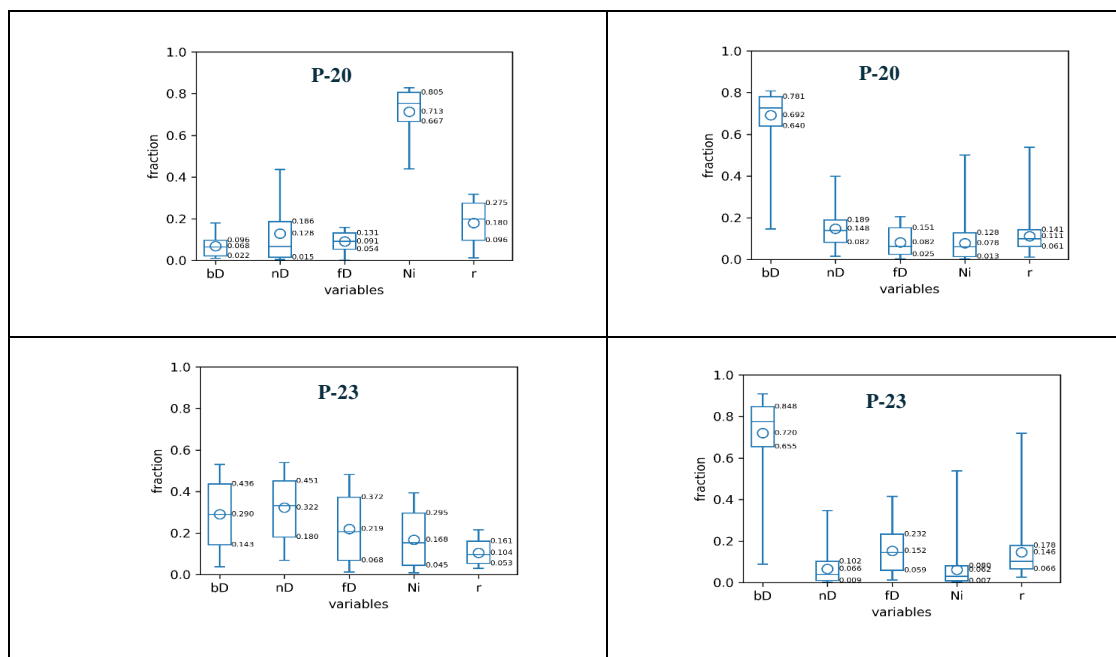
653 After glucose addition, the isotopic data indicate that N_2O production was primarily driven by
654 bacterial denitrification (bD), with relatively low $\delta^{15}\text{N}^{\text{SP}}_{\text{N}_2\text{O}}$ and $\delta^{18}\text{O}_{\text{N}_2\text{O}}$ values, clustering mostly
655 around reduction line. In the $\delta^{15}\text{N}^{\text{SP}}$ - $\delta^{15}\text{N}$ space, mostly the isotopic data showed a clear shift
656 toward bD, supported by a significant increase in $\delta^{15}\text{N}_{\text{N}_2\text{O}}$ values, indicating N_2O production from
657 the slightly ^{15}N -labeled NO_3^- pool and some effect of N_2O reduction. In P-23, however, the data
658 indicate more possible pathways mixture, including nitrification (Ni) and fungal denitrification
659 (fD). Significant reduction of N_2O to N_2 can be supposed based on the clustering of the points
660 along the N_2O reduction line, especially in the $\delta^{15}\text{N}^{\text{SP}}$ - $\delta^{18}\text{O}$ isotope map, Fig. 5). In $\delta^{15}\text{N}^{\text{SP}}$ - $\delta^{15}\text{N}$



661 isotope map the effect of N₂O reduction is less visible, because the artificially elevated δ¹⁵N values
 662 result in very steep reduction line. Minimal clustering near the fungal denitrification (fD) zone
 663 suggests limited fungal contributions to N₂O production. However, the δ¹⁵N^{SP}- δ¹⁸O map shows
 664 some samples near the fD zone (Fig. 5A), and the FRAME model (Fig. 8) also supports this with
 665 minor yet detectable fungal involvement. The shift in δ¹⁵N^{SP}_{N₂O} values also reflects the changing
 666 dynamics, with nitrification and nitrifier denitrification becoming less prominent as bacterial
 667 denitrification intensified. In conclusion, the isotopic data demonstrate that carbon availability
 668 strongly influenced the balance between N₂O production and reduction, driving microbial N
 669 transformations and regulating N₂O emissions during laboratory incubation.
 670 These isotope results of N₂O from the headspace samples were jointly analyzed using the three
 671 dimensional FRAME (FRActionation and Mixing Evaluation) model (Lewicki et al., 2022) to
 672 quantitatively interpret the isotopic signatures of N₂O, identifying microbial pathways driving N₂O
 673 production and estimating N₂O reduction progress. This offers most precise insight into N
 674 transformations under controlled experimental conditions.

675
 676
 677





678
 679 **Figure 8: N₂O production pathways contribution and N₂O reduction progress based on the**
 680 **FRAME modelling of the experimental N₂O isotope data collected for the first analysed**
 681 **samples (before glucose addition, 1st and 2nd sampling, day 2 and 4) (A) and mean value of**
 682 **the later samples (after glucose addition, 4th and 5th sampling, day 9 and 11) (B).** The estimated
 683 contributions of bacterial denitrification (bd), nitrifier denitrification (nD), fungal denitrification
 684 (fD), and autotrophic nitrification (Ni) illustrate the dynamic shifts in microbial pathways and N₂O
 685 reduction progress (r) over time.

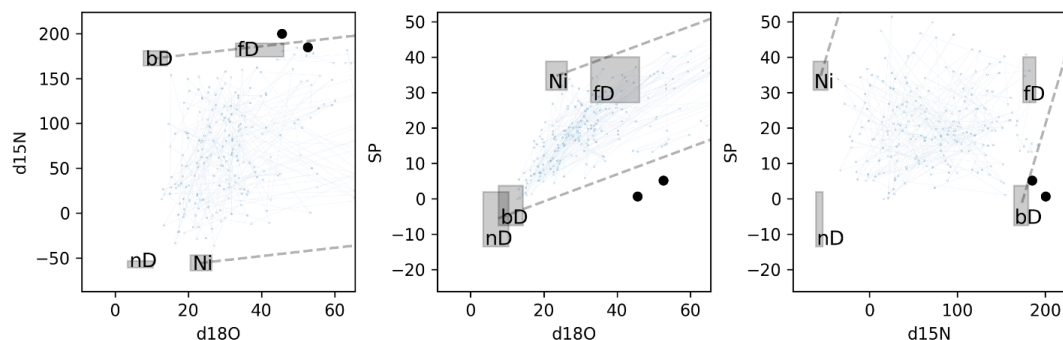
686
 687 The graphs, analyzed using the FRAME model, reveal distinct microbial processes driving N₂O
 688 production and reduction during laboratory incubation of groundwater samples from piezometers
 689 P-7, P-16, P-20, and P-23, comparing the initial incubation phase (1–2 days) to the later phase (4–
 690 14 days), including samples before and after glucose addition.

691 This division of samples was made after the observed isotopic signatures – the initial samples (day
 692 2) showed no ¹⁵N enrichment in the N₂O and later samples (day 7 – day 14) were characterised
 693 with very significant ¹⁵N enrichment. Initially, autotrophic nitrification (Ni) dominated across all
 694 samples, contributing around 60–70% to N₂O production, while bacterial denitrification (bd) was
 695 lower, ranging between 20–30%. In P-7 and P-16, minor contributions from nitrifier denitrification
 696 (nD) (10–20%) and fungal denitrification (fD) (<10%) were observed, with similar trends in P-20
 697 and P-23, where nD accounted for slightly higher fractions of N₂O production. Residual N₂O
 698 fractions (r_{N2O}) across all piezometers ranged between 10–26%, reflecting high partial N₂O
 699 reduction to N₂.

700 After glucose addition, microbial activity shifted significantly toward denitrification, with bd
 701 becoming the dominant pathway (up to 80–85%), driven by the availability of carbon. P-7 and P-



702 16 exhibited a gradual rise in bD, reaching up to 73%, while residual Ni contributions declined
703 correspondingly. In P-20 and P-23, the transition was sharper, with bD dominance occurring more
704 abruptly. Residual N₂O fractions decreased across all samples as bD activity intensified.
705 Simultaneously, Ni contributions dropped below 10% in all samples, while nD and fD remained
706 minimal, contributing <15% to N₂O production. Interestingly, for the last sample (day 14 of the
707 incubation) for all the analysed waters the model could not find any solution. This might be due
708 to accumulation of very different pathways contribution and progressing reduction of N₂O
709 originating from the mixture of all production pathways. Figure 9 presents illustration of the model
710 performance on an example of sample 6 (day 14) of the P-16, while this is similar for all the
711 piezometers. The modelling problem occurs due to too high $\delta^{18}\text{O}$ measured values, while $\delta^{15}\text{N}$ and
712 $\delta^{15}\text{N}^{\text{SP}}$ show values typical for bD, $\delta^{18}\text{O}$ is shifted to much higher values, indicating large
713 reduction, not confirmed with low $\delta^{15}\text{N}^{\text{SP}}$ values. This can result from the actual smaller O-isotope
714 exchange with water than the one assumed by for bD in the model input values. The endmember
715 values for bD are mostly determined based on soil experimental studies (Yu et al., 2020), hence it
716 is theoretically possible that slightly different range of values should be assumed for groundwater
717 studies. Another explanation could be significant admixture of chemodenitrification, which is
718 characterized by high $\delta^{18}\text{O}$ values ((Wei et al., 2019). This assumption might be supported by the
719 fact that quite significant N₂O production was found in some of sterile samples, with especially
720 high production at the end of the experiment (Table 2). This N₂O produced from sterile treatments
721 shows always high $\delta^{18}\text{O}$ values and very variable $\delta^{15}\text{N}^{\text{SP}}$ values (Fig. 5A).
722 This interpretation is further supported by the elevated $\delta^{18}\text{O}$ values in later incubation stages,
723 suggesting abiotic processes like chemodenitrification which may have contributed to N₂O
724 production. Chemodenitrification has been shown to produce N₂O with distinct isotope
725 fractionation patterns, including elevated $\delta^{18}\text{O}$ values compared to microbial pathways (Chen et
726 al., 2021). The detection of N₂O in sterile samples also points to a possible non-biological
727 contribution, as nitrite can undergo chemical reduction in the absence of microbial activity (Heil
728 et al., 2016). Furthermore, abiotic N₂O formation has been linked to Fe(II)-mediated nitrite
729 reduction, particularly under anoxic conditions, with organic matter, including humic and fulvic
730 acids, potentially facilitating N₂O production through chemical pathways (Zhu-Barker et al.,
731 2015). However, since Fe(II) presence in our sterile samples is unknown, other abiotic
732 mechanisms, such as organic matter interactions, cannot be ruled out.
733 Importantly, the FRAME model does not include chemodenitrification, which is most probably
734 the reason for biased results for the last samples. The discrepancies between modeled and observed
735 isotope values suggest that additional abiotic pathways, such as chemodenitrification, may need to
736 be considered in future isotope models to improve accuracy.
737



738
739 **Figure 9: An example of the FRAME modelling path illustration for the last incubation**
740 **samples (P-16, day 14), which do not provide modelling results.** The black dots illustrate
741 measured samples and the blue points the model Monte Carlo sampling. No coherence of measured
742 and modelled data indicate that the model did not find plausible solution for the given data.

743
744 All piezometers displayed a similar transition from nitrification-driven processes in the first
745 samples to denitrification-dominated processes in the later incubation days. However, at the final
746 sampling points, no fitted solution could be obtained for some data, suggesting the presence of
747 unknown processes or a complex overlap of microbial pathways. These findings indicate very
748 dynamic N₂O production processes while highlighting limitations in resolving mixed nitrogen
749 pathways at later stages. Moreover, while microbial denitrification was the primary N₂O source,
750 the observed discrepancies suggest that abiotic contributions, such as chemodenitrification, may
751 have been a more relevant factor than initially expected, particularly under conditions favoring
752 nitrite accumulation.

753 754 **4.2.3 Gene Abundance Shifts in Microbial Communities**

755 Pre-incubation data indicate a notable presence of archaeal *amoA* genes compared to bacterial
756 *amoA*, suggesting active archaeal ammonia oxidation in the samples (Fig. 6A). While
757 denitrification gene *nosZI*—show relatively high abundance in some samples (e.g., P-16 and P-
758 23), the consistent presence of archaeal *amoA* and the lower abundance of other denitrification-
759 related genes (*nirK*, *nirS*), , suggests nitrification processes were prominent prior to incubation.
760 This is particularly evident in P-7 and P-20, where archaeal *amoA* surpasses denitrification genes,
761 suggesting a stronger nitrification potential.

762 This is consistent with findings from (Mosley et al., 2022), which reported that ammonia-oxidizing
763 archaea (AOA) tend to dominate in oligotrophic groundwater environments with low ammonia
764 concentrations due to their higher affinity for ammonia and oxygen limitation, often outnumbering
765 ammonia-oxidizing bacteria (AOB). Similarly, the functional gene proportion analysis (Fig. 6B)
766 highlight the contribution of archaeal *amoA* genes to total prokaryotic abundance, emphasizing
767 their critical role in ammonia oxidation.. In contrast, the low proportions of bacterial *amoA* further
768 confirm limited bacterial involvement in N cycling prior to incubation. This has also been observed
769 in groundwater systems where bacterial nitrification potential remains constrained due to
770 environmental limitations on AOB populations. Post-incubation, there was a significant increase



771 in the abundance of denitrification genes like *nosZI*, particularly in samples P-7, P-16 and P-20,
772 illustrating a shift from nitrification to denitrification under incubation conditions Fig. 6(A). This
773 aligns with (Wang et al., 2022), who found that site-specific environmental conditions, particularly
774 carbon and N availability drive microbial community shifts in N cycling, with increased
775 denitrification gene abundance. Functional gene proportions also reveal a corresponding rise in the
776 relative abundance of *nosZI*, illustrating the shift in microbial community function towards
777 denitrification processes Fig. 6(B). The abundance of DNRA and commamox genes showed
778 minimal changes, suggesting no difference in the presence of these processes between pre- and
779 post-incubation conditions. This observation is supported by (Broman et al., 2021), who reported
780 that DNRA gene abundance remained stable under experimental conditions, indicating its potential
781 resilience to shifts in N cycling pathway. The abundance of archaeal 16S rRNA genes decreased
782 in samples P-7 and P-23, indicating a reduction in archaeal community, whereas the abundance of
783 bacterial 16S rRNA increased significantly in P-16 and P-20, reflecting bacterial growth during
784 incubation. Paired T-tests confirmed these observations, showing significant increases in the
785 abundance of *nosZI* genes in P7 ($p < 0.05$) and P16 ($p < 0.05$) and shifts in the archaeal 16S rRNA
786 abundance ($p < 0.05$), but not in the abundances of *nirK* or *nosZII* genes ($p > 0.05$), highlighting the
787 variability in microbial responses. These results suggest that specific environmental or
788 experimental conditions during incubation can significantly influence certain microbial processes,
789 particularly those related to N cycling. This is consistent with (Wang et al., 2022), who found N-
790 cycling gene abundance varies with environmental factors like carbon and N availability.
791 Similarly, (Mosley et al., 2022) reported persistent transcriptional activity in nitrification and
792 denitrification across groundwater conditions, indicating microbial adaptability. The significant
793 results for the community of *nosZI* and archaeal 16s rRNA highlight their potential roles in
794 environmental monitoring and microbial ecology studies.

795

796 **4.2.4 The identification of active N transformations in the laboratory incubations**

797 The interpretation of the presented results is quite challenging, since this is the first study
798 combining the N and O isotope analyses of NO_3^- and NO_2^- as well as N_2O isotopes including three
799 signatures: $\delta^{15}\text{N}_{\text{N}_2\text{O}}^{\text{SP}}$, $\delta^{18}\text{O}_{\text{N}_2\text{O}}$ and $\delta^{15}\text{N}_{\text{N}_2\text{O}}$. The overall summary of this data is rather surprising
800 and may seem inconsistent, because the low-level ^{15}N label added to the NO_3^- pool is not found in
801 the NO_2^- pool, but almost completely transferred to the N_2O pool. Both the N_2O isotope results
802 and gene copy numbers document occurrence of intensive denitrification, especially in the second
803 phase of the incubation, whereas the analyses of inorganic N indicate simultaneous intensive
804 nitrification processes, with significant formation of NO_2^- . It is surprising due to very low levels of
805 NH_4^+ during the whole incubation and indicates that the additional unlabelled N must originate
806 from organic nitrogen pool (DON).

807 The FRAME analysis of N_2O isotope data, T-test results, and gene abundance graphs together
808 show a shift from nitrification to denitrification in microbes during incubation, influenced by
809 adding carbon source and created suboxic conditions. Initially, the FRAME results show that
810 nitrification, mainly due to archaeal community (as seen with high levels of the archaeal *amoA*



811 gene), is the dominant N₂O production pathway. Isotope analysis supports this, with N₂O isotope
812 signatures characteristic for nitrification for the first samples (Fig. 5, Fig.8). Pre-incubation data
813 indicate that archaeal ammonia oxidation was a dominant process in samples P-7 and P-20, as
814 evidenced by higher archaeal *amoA* gene abundance relative to denitrification-related genes.
815 However, in samples such as P-16 and P-23, the abundance of *nosZI* suggests that denitrification
816 processes were also active, pointing to a co-occurrence of nitrification and denitrification processes
817 across the groundwater samples.

818 Post-incubation, FRAME results show an increase in bacterial denitrification (bD) fractions,
819 correlating with the significant rise in denitrification-related genes, particularly *nosZI* validated by
820 paired T-tests ($p < 0.05$). These changes are confirmed by gene abundance graphs that show a
821 notable increase in these denitrification genes after incubation. The total prokaryotic abundance
822 also increased in P-16 and P-20, reflecting enhanced bacterial growth, whereas smaller changes in
823 P-7 and P-23 suggest variable responses to carbon addition (Fig. 6). A decline in nitrification genes
824 align with the FRAME-predicted reduction in nitrification activity. Additionally, isotopic data
825 revealed significant N₂O reduction to N₂ in most samples, consistent with bacterial denitrification
826 dominance, reduced contributions from nitrification pathways, and increase in the abundance of
827 genes responsible for N₂O reduction to N₂ (*nosZII*). Together, these results confirm microbial
828 transition from archaeal-driven nitrification to bacterial denitrification, highlight the role of carbon
829 availability and suboxic conditions in regulating N cycling. The integration of gene abundance,
830 isotope dynamics, and FRAME analysis provides a comprehensive understanding of the microbial
831 processes driving N transformations during incubation.

832 Importantly, the overall results showed that both reduction and oxidation processes are occurring
833 simultaneously in the studied aquifer. Theoretically, in our incubations the suboxic conditions
834 should rather favor denitrification NO₃⁻ reduction. Indeed, the majority of the released N₂O is
835 formed due to bacterial denitrification from NO₃⁻ as a substrate. However, NO₂⁻ originate in large
836 majority from organic N oxidation with very minor fraction originating from NO₃⁻ reduction.

837 **5. Conclusions and outlook**

838 This study demonstrates the intricate dynamics of N transformations in groundwater samples by
839 integrating isotope analyses, microbial gene abundance, and FRAME modeling to elucidate the
840 microbial mechanisms involved. Application of multi-compound isotope studies (NO₃⁻, NO₂⁻,
841 N₂O) combined with the novel idea of low-level ¹⁵N labelling and microbiome studies provide a
842 very detailed insight into the occurring processes and reveal some unexpected mechanisms. Based
843 on this complex dataset we can document the co-occurrence of the oxidation and reduction
844 pathways and existence of different, separated NO₂⁻ pools.

845 NO₂⁻ production is likely driven by nitrification processes linked to the oxidation of organic N
846 from the elevated DON levels in water samples. Also, the data indicated the simultaneous
847 occurrence of denitrification processes, particularly under suboxic conditions induced during



848 incubation, highlighting the dynamic nature of nitrogen cycling. Future investigations into the role
849 of DON could deepen understanding of its impact on nitrification and denitrification in waters.
850 Broader application of these integrated methods combining isotope analyses and microbial gene
851 studies in field-scale studies can improve monitoring and management of nitrogen pollution in
852 groundwater systems.

853 **6. Data availability**

854 Original data are available upon request. Material necessary for this study's findings is presented
855 in the paper.

856 **7. Author contribution**

857 Conceptualization was led by SD, with supervision from DLS and ME. Visualization (figures and
858 plots) prepared by SD and DLS. Microbiological analyses were conducted by SD and ME. SD,
859 DLS contributed to writing, methodology, investigation, data curation. Fieldwork and sample
860 collection were carried out by SD, DLS, MB, and MJ. Funding acquisition and resources were
861 supported by SD, DLS, ME and UM. Gas and isotope analyses were performed by SD, DLS, and
862 RW. We thank all our co-authors for their valuable support and feedback.

863 **8. Competing interest**

864 The authors declare that they have no conflict of interest.

865 **8. Financial support**

866 This study was financially supported by the “Polish Returns” programme of the Polish National
867 Agency of Academic Exchange and the grants Opus-516204 (PI: Dominika Lewicka-Szczebak)
868 624 and Preludium-522855 (PI: Sushmita Deb) of the National Science Centre Poland. Also,
869 supported by the Estonian Research Council (PRG2032), by the European Union Horizon program
870 under grant agreement No 101079192 (MLTOM23003R), and the European Research Council
871 (ERC) under grant agreement No 101096403 (MLTOM23415R).

872

873

874

875

876



877 7. References

- 878 Böhlke, J.K., Smith, R.L., Hannon, J.E., 2007. Isotopic Analysis of N and O in Nitrite and
879 Nitrate by Sequential Selective Bacterial Reduction to N₂O. *Anal Chem* 79, 5888–5895.
880 <https://doi.org/10.1021/ac070176k>
- 881 Boumaiza, L., Stotler, R.L., Mayer, B., Matiatos, I., Sacchi, E., Otero, N., Johannesson, K.H.,
882 Huneau, F., Chesnaux, R., Blarasin, M., Re, V., Knöller, K., 2024. How the $\delta^{18}\text{O}_{\text{NO}_3}$
883 versus $\delta^{15}\text{N}_{\text{NO}_3}$ Plot Can Be Used to Identify a Typical Expected Isotopic Range of
884 Denitrification for NO₃-Impacted Groundwaters. *ACS ES&T Water* 4, 5243–5254.
885 <https://doi.org/10.1021/acsestwater.4c00796>
- 886 Brettar, I., Sanchez-Perez, J.-M., Trémolières, M., 2002. Nitrate elimination by denitrification in
887 hardwood forest soils of the Upper Rhine floodplain - Correlation with redox potential and
888 organic matter. *Hydrobiologia* 469, 11–21. <https://doi.org/10.1023/A:1015527611350>
- 889 Broman, E., Zilius, M., Samuiloviene, A., Vybernaite-Lubiene, I., Politi, T., Klawonn, I., Voss,
890 M., Nascimento, F.J.A., Bonaglia, S., 2021. Active DNRA and denitrification in oxic
891 hypereutrophic waters. *Water Res* 194. <https://doi.org/10.1016/j.watres.2021.116954>
- 892 Bucha, M., Lewicka-Szczebak, D., Wójtowicz, P., 2025. Simultaneous measurement of
893 greenhouse gases (CH₄, CO₂ and N₂O) at atmospheric levels using a gas chromatography
894 system. *Atmos Meas Tech* 1–16.
- 895 Buchen-Tschiskale, C., Well, R., Flessa, H., 2023. Tracing nitrogen transformations during
896 spring development of winter wheat induced by ¹⁵N labeled cattle slurry applied with
897 different techniques. *Science of The Total Environment* 871, 162061.
898 <https://doi.org/10.1016/j.scitotenv.2023.162061>
- 899 Butterbach-Bahl, K., Baggs, E.M., Dannenmann, M., Kiese, R., Zechmeister-Boltenstern, S.,
900 2013. Nitrous oxide emissions from soils: how well do we understand the processes and
901 their controls? *Philosophical Transactions of the Royal Society B: Biological Sciences* 368,
902 20130122. <https://doi.org/10.1098/rstb.2013.0122>
- 903 Chen, G., Zhao, W., Yang, Y., Chen, D., Wang, Y., Li, F., Zhao, Z., Cao, F., Liu, T., 2021.
904 Chemodenitrification by Fe(II) and nitrite: Effects of temperature and dual N[sbnd]O
905 isotope fractionation. *Chem Geol* 575. <https://doi.org/10.1016/j.chemgeo.2021.120258>
- 906 Clague, J.C., Stenger, R., Morgenstern, U., 2019. The influence of unsaturated zone drainage
907 status on denitrification and the redox succession in shallow groundwater. *Science of The*
908 *Total Environment* 660, 1232–1244. <https://doi.org/10.1016/j.scitotenv.2018.12.383>
- 909 Cui, Y.-X., Biswal, B.K., Guo, G., Deng, Y.-F., Huang, H., Chen, G.-H., Wu, D., 2019.
910 Biological nitrogen removal from wastewater using sulphur-driven autotrophic
911 denitrification. *Appl Microbiol Biotechnol* 103, 6023–6039. [https://doi.org/10.1007/s00253-](https://doi.org/10.1007/s00253-019-09935-4)
912 [019-09935-4](https://doi.org/10.1007/s00253-019-09935-4)
- 913 Deb, S., Lewicka-Szczebak, D., Rohe, L., 2024. Microbial nitrogen transformations tracked by
914 natural abundance isotope studies and microbiological methods: A review. *Science of The*
915 *Total Environment* 926, 172073. <https://doi.org/10.1016/j.scitotenv.2024.172073>
- 916 Denk, T.R.A., Mohn, J., Decock, C., Lewicka-Szczebak, D., Harris, E., Butterbach-Bahl, K.,
917 Kiese, R., Wolf, B., 2017. The nitrogen cycle: A review of isotope effects and isotope
918 modeling approaches. *Soil Biol Biochem*. <https://doi.org/10.1016/j.soilbio.2016.11.015>
- 919 Ding, B., Li, Z., Cai, M., Lu, M., Liu, W., 2022. Feammox is more important than anammox in
920 anaerobic ammonium loss in farmland soils around Lake Taihu, China. *Chemosphere* 305,
921 135412. <https://doi.org/10.1016/j.chemosphere.2022.135412>



- 922 Einsiedl, F., Wunderlich, A., Sebiló, M., Coskun, Ö.K., Orsi, W.D., Mayer, B., 2020.
923 Biogeochemical evidence of anaerobic methane oxidation and anaerobic ammonium
924 oxidation in a stratified lake using stable isotopes. *Biogeosciences* 17, 5149–5161.
925 <https://doi.org/10.5194/bg-17-5149-2020>
- 926 Espenberg, M., Pille, K., Yang, B., Maddison, M., Abdalla, M., Smith, P., Li, X., Chan, P.-L.,
927 Mander, Ü., 2024. Towards an integrated view on microbial CH₄, N₂O and N₂ cycles in
928 brackish coastal marsh soils: A comparative analysis of two sites. *Science of The Total*
929 *Environment* 918, 170641. <https://doi.org/10.1016/j.scitotenv.2024.170641>
- 930 Espenberg, M., Truu, M., Mander, Ü., Kasak, K., Nölvak, H., Ligi, T., Oopkaup, K., Maddison,
931 M., Truu, J., 2018. Differences in microbial community structure and nitrogen cycling in
932 natural and drained tropical peatland soils. *Sci Rep* 8, 4742. <https://doi.org/10.1038/s41598-018-23032-y>
- 933
- 934 Harris, S. J., Liisberg, J., Xia, L., Wei, J., Zeyer, K., Yu, L., Barthel, M., Wolf, B., Kelly, B. F.
935 J., Cendón, D. I., Blunier, T., Six, J., and Mohn, J., 2020. N₂O isotopocule measurements
936 using laser spectroscopy: analyzer characterization and intercomparison, *Atmos. Meas.*
937 *Tech.*, 13, 2797–2831, <https://doi.org/10.5194/amt-13-2797-2020>.
- 938 Heil, J., Vereecken, H., Brüggemann, N., 2016. A review of chemical reactions of nitrification
939 intermediates and their role in nitrogen cycling and nitrogen trace gas formation in soil. *Eur*
940 *J Soil Sci.* <https://doi.org/10.1111/ejss.12306>
- 941 Hommes, N.G., Sayavedra-Soto, L.A., Arp, D.J., 2003. Chemolithoorganotrophic Growth of
942 *Nitrosomonas europaea* on Fructose. *J Bacteriol* 185, 6809–6814.
943 <https://doi.org/10.1128/JB.185.23.6809-6814.2003>
- 944 Hu, J., Tian, J., Deng, X., Liu, X., Zhou, F., Yu, J., Chi, R., Xiao, C., 2024. Heterotrophic
945 nitrification processes driven by glucose and sodium acetate: New insights into microbial
946 communities, functional genes and nitrogen metabolism from metagenomics and
947 metabolomics. *Bioresour Technol* 408, 131226.
948 <https://doi.org/10.1016/j.biortech.2024.131226>
- 949 Kuusemets, L., Mander, Ü., Escuer-Gatius, J., Astover, A., Kauer, K., Soosaar, K., Espenberg,
950 M., 2024. Interactions of fertilisation and crop productivity on soil nitrogen cycle
951 microbiome and gas emissions. <https://doi.org/10.5194/egusphere-2024-593>
- 952 Levy-Booth, D.J., Prescott, C.E., Grayston, S.J., 2014. Microbial functional genes involved in
953 nitrogen fixation, nitrification and denitrification in forest ecosystems. *Soil Biol Biochem*
954 75, 11–25. <https://doi.org/10.1016/j.soilbio.2014.03.021>
- 955 Lewicka-Szczebak, D., Jansen-Willems, A., Müller, C., Dyckmans, J., Well, R., 2021. Nitrite
956 isotope characteristics and associated soil N transformations. *Sci Rep* 11, 5008.
957 <https://doi.org/10.1038/s41598-021-83786-w>
- 958 Lewicka-Szczebak, D., Lewicki, M.P., Well, R., 2020. N₂O isotope approaches for source
959 partitioning of N₂O production and estimation of N₂O reduction – validation with the 15N
960 gas-flux method in laboratory and field studies. *Biogeosciences* 17, 5513–5537.
961 <https://doi.org/10.5194/bg-17-5513-2020>
- 962 Lewicki, M.P., Lewicka-Szczebak, D., Skrzypek, G., 2022. FRAME—Monte Carlo model for
963 evaluation of the stable isotope mixing and fractionation. *PLoS One* 17, e0277204.
964 <https://doi.org/10.1371/journal.pone.0277204>
- 965 MASTA, M., ESPENBERG, M., KUUSEMETS, L., PÄRN, J., THAYAMKOTTU, S., SEPP,
966 H., KIRSIMÄE, K., SGOURIDIS, F., KASAK, K., SOOSAAR, K., MANDER, Ü., 2024.
967 15N tracers and microbial analyses reveal in situ N₂O sources in contrasting water regimes



- 968 of a drained peatland forest. *Pedosphere* 34, 749–758.
969 <https://doi.org/10.1016/j.pedsph.2023.06.006>
- 970 Mohn, J., Wolf, B., Toyoda, S., Lin, C.T., Liang, M.C., Brüggemann, N., Wissel, H., Steiker,
971 A.E., Dyckmans, J., Szewc, L., Ostrom, N.E., Casciotti, K.L., Forbes, M., Giesemann, A.,
972 Well, R., Doucett, R.R., Yarnes, C.T., Ridley, A.R., Kaiser, J., Yoshida, N., 2014.
973 Interlaboratory assessment of nitrous oxide isotopomer analysis by isotope ratio mass
974 spectrometry and laser spectroscopy: Current status and perspectives. *Rapid*
975 *Communications in Mass Spectrometry* 28, 1995–2007. <https://doi.org/10.1002/rcm.6982>
- 976 Moore, K.B., Ekwurzel, B., Esser, B.K., Hudson, G.B., Moran, J.E., 2006. Sources of
977 groundwater nitrate revealed using residence time and isotope methods. *Applied*
978 *Geochemistry* 21, 1016–1029. <https://doi.org/10.1016/j.apgeochem.2006.03.008>
- 979 Mosley, O.E., Gios, E., Close, M., Weaver, L., Daughney, C., Handley, K.M., 2022. Nitrogen
980 cycling and microbial cooperation in the terrestrial subsurface. *ISME Journal* 16, 2561–
981 2573. <https://doi.org/10.1038/s41396-022-01300-0>
- 982 Müller, C., Laughlin, R.J., Spott, O., Rütting, T., 2014. Quantification of N₂O emission
983 pathways via a ¹⁵N tracing model. *Soil Biol Biochem* 72, 44–54.
984 <https://doi.org/10.1016/j.soilbio.2014.01.013>
- 985 Müller, C., Stevens, R.J., Laughlin, R.J., 2004. A ¹⁵N tracing model to analyse N
986 transformations in old grassland soil. *Soil Biol Biochem* 36, 619–632.
987 <https://doi.org/10.1016/j.soilbio.2003.12.006>
- 988 Nikolenko, O., Jurado, A., Borges, A. V., Knöller, K., Brouyère, S., 2018. Isotopic composition
989 of nitrogen species in groundwater under agricultural areas: A review. *Science of the Total*
990 *Environment*. <https://doi.org/10.1016/j.scitotenv.2017.10.086>
- 991 Olichwer, T., Wcisło, M., Staśko, S., Buczyński, S., Modelska, M., Tarka, R., 2012. Numerical
992 Model Of The Catchments Of The Oziąbel And Wolczyński Strumień Rivers-Wolczyn
993 Municipality, *Studia Geotechnica et Mechanica*.
- 994 Rohe, L., Oppermann, T., Well, R., Horn, M.A., 2020. Nitrite induced transcription of p450_{nor}
995 during denitrification by *Fusarium oxysporum* correlates with the production of N₂O with a
996 high ¹⁵N site preference. *Soil Biol Biochem* 151, 108043.
997 <https://doi.org/10.1016/j.soilbio.2020.108043>
- 998 Rütting, T., Aronsson, H., Delin, S., 2018. Efficient use of nitrogen in agriculture. *Nutr Cycl*
999 *Agroecosyst*. <https://doi.org/10.1007/s10705-017-9900-8>
- 1000 Rütting, T., Müller, C., 2008. Process-specific analysis of nitrite dynamics in a permanent
1001 grassland soil by using a Monte Carlo sampling technique. *Eur J Soil Sci* 59, 208–215.
1002 <https://doi.org/10.1111/j.1365-2389.2007.00976.x>
- 1003 Sainju, M., U., Ghimire, R., P. Pradhan, G., 2020. Nitrogen Fertilization I: Impact on Crop, Soil,
1004 and Environment, in: *Nitrogen Fixation*. IntechOpen.
1005 <https://doi.org/10.5772/intechopen.86028>
- 1006 Sigman, D.M., Casciotti, K.L., Andreani, M., Barford, C., Galanter, M., Böhlke, J.K., 2001. A
1007 bacterial method for the nitrogen isotopic analysis of nitrate in seawater and freshwater.
1008 *Anal Chem* 73, 4145–4153. <https://doi.org/10.1021/ac010088e>
- 1009 Wang, P., Li, J.L., Luo, X.Q., Ahmad, M., Duan, L., Yin, L.Z., Fang, B.Z., Li, S.H., Yang, Y.,
1010 Jiang, L., Li, W.J., 2022. Biogeographical distributions of nitrogen-cycling functional genes
1011 in a subtropical estuary. *Funct Ecol* 36, 187–201. <https://doi.org/10.1111/1365-2435.13949>
- 1012 Wang, X., Wells, N.S., Xiao, W., Hamilton, J.L., Jones, A.M., Collins, R.N., 2022. Mackinawite
1013 (FeS) Chemodenitrification of Nitrate (NO₃⁻) under Acidic to Neutral pH Conditions and



- 1014 Its Stable N and O Isotope Dynamics. *ACS Earth Space Chem* 6, 2801–2811.
1015 <https://doi.org/10.1021/acsearthspacechem.2c00158>
1016 Watanabe, Y., Aoki, W., Ueda, M., 2023. Ammonia Production Using Bacteria and Yeast
1017 toward a Sustainable Society. *Bioengineering* 10, 82.
1018 <https://doi.org/10.3390/bioengineering10010082>
1019 Wei, J., Ibraim, E., Brüggemann, N., Vereecken, H., Mohn, J., 2019. First real-time isotopic
1020 characterisation of N₂O from chemodenitrification. *Geochim Cosmochim Acta* 267, 17–32.
1021 <https://doi.org/10.1016/j.gca.2019.09.018>
1022 Well, R., Burkart, S., Giesemann, A., Grosz, B., Köster, J.R., Lewicka-Szczebak, D., 2019.
1023 Improvement of the ¹⁵N gas flux method for *in situ* measurement of soil denitrification and
1024 its product stoichiometry. *Rapid Communications in Mass Spectrometry* 33, 437–448.
1025 <https://doi.org/10.1002/rcm.8363>
1026 Wolters, T., Bach, T., Eisele, M., Eschenbach, W., Kunkel, R., McNamara, I., Well, R.,
1027 Wendland, F., 2022. The derivation of denitrification conditions in groundwater: Combined
1028 method approach and application for Germany. *Ecol Indic* 144, 109564.
1029 <https://doi.org/10.1016/J.ECOLIND.2022.109564>
1030 Yu, L., Harris, E., Lewicka-Szczebak, D., Barthel, M., Blomberg, M.R.A., Harris, S.J., Johnson,
1031 M.S., Lehmann, M.F., Liisberg, J., Müller, C., Ostrom, N.E., Six, J., Toyoda, S., Yoshida,
1032 N., Mohn, J., 2020. What can we learn from N₂O isotope data? – Analytics, processes and
1033 modelling. *Rapid Communications in Mass Spectrometry* 34.
1034 <https://doi.org/10.1002/rcm.8858>
1035 Zhang, Y., Cai, Z., Zhang, J., Müller, C., 2023. The controlling factors and the role of soil
1036 heterotrophic nitrification from a global review. *Applied Soil Ecology* 182, 104698.
1037 <https://doi.org/10.1016/j.apsoil.2022.104698>
1038 Zheng, J., Fujii, K., Koba, K., Wanek, W., Müller, C., Jansen-Willems, A.B., Nakajima, Y.,
1039 Wagai, R., Canarini, A., 2023. Revisiting process-based simulations of soil nitrite
1040 dynamics: Tighter cycling between nitrite and nitrate than considered previously. *Soil Biol*
1041 *Biochem* 178, 108958. <https://doi.org/10.1016/j.soilbio.2023.108958>
1042 Zhu-Barker, X., Cavazos, A.R., Ostrom, N.E., Horwath, W.R., Glass, J.B., 2015. The importance
1043 of abiotic reactions for nitrous oxide production. *Biogeochemistry* 126, 251–267.
1044 <https://doi.org/10.1007/s10533-015-0166-4>

1045

1046